J. Membrane Biol. 184, 143–159 (2001)
DOI: 10.1007/s00232-001-0083-4

The Journal of
Membrane
Biology

State-Dependent Inhibition of Inactivation-Deficient $Ca_V1.2$ and $Ca_V2.3$ Channels By Mibefradil

G. Bernatchez, R. Sauvé, L. Parent
Department of Physiology, Membrane Transport Research Group, Université de Montréal, P.O. Box 6128, Downtown Station, Montréal, Qué, H3C 3J7, Canada

Received: 14 March 2001/Revised: 25 June 2001

Abstract. The structural determinants of mibefradil inhibition were analyzed using wild-type and inactivation-modified $Ca_V1.2$ (α1C) and $Ca_V2.3$ (α1E) channels. Mibefradil inhibition of peak Ba^{2+} currents was dose- and voltage-dependent. An increase of holding potentials from −80 to −100 mV significantly shifted dose-response curves toward higher mibefradil concentrations, namely from a concentration of 108 ± 21 μM ($n = 7$) to 288 ± 17 μM ($n = 3$) for inhibition of half of the $Ca_v1.2$ currents (IC_{50}) and from $IC_{50} = 8 \pm 2$ μM ($n = 9$) to 33 ± 7 μM ($n = 4$) for $Ca_V2.3$ currents. In the presence of mibefradil, $Ca_V1.2$ and $Ca_V2.3$ experienced significant use-dependent inhibition (0.1 to 1 Hz) and slower recovery from inactivation suggesting mibefradil could promote transition(s) to an absorbing inactivated state. In order to investigate the relationship between inactivation and drug sensitivity, mibefradil inhibition was studied in inactivation-altered $Ca_V1.2$ and $Ca_V2.3$ mutants. Mibefradil significantly delayed the onset of channel recovery from inactivation in CEEE (Repeat I + part of the I–II linker from $Ca_V1.2$ in the $Ca_V2.3$ host channel), in EC(*AID*)EEE (part of the I–II linker from $Ca_V1.2$ in the $Ca_V2.3$ host channel) as well as in $Ca_V1.2$ E462R, and $Ca_V2.3$ R378E (point mutation in the β-subunit binding motif) channels. Mibefradil inhibited the faster inactivating chimera EC(*IS1-6*)EEE with an $IC_{50} = 7 \pm 1$ μM ($n = 3$), whereas the slower inactivating chimeras EC(*AID*)EEE and CEEE were, respectively, inhibited with $IC_{50} = 41 \pm 5$ μM ($n = 4$) and $IC_{50} = 68 \pm 9$ μM ($n = 5$). Dose-response curves were superimposable for the faster EC(*IS1-6*)EEE and $Ca_V2.3$, whereas intermediate-inactivating channel kinetics (CEEE, $Ca_V1.2$ E462R, and $Ca_V1.2$ E462K) were inhibited by similar concentrations of mibefradil with $IC_{50} \approx 55$–75 μM. The slower $Ca_V1.2$ wild-type and $Ca_V1.2$ Q473K channels responded to higher doses of mibefradil with $IC_{50} \approx 100$–120 μM. Mibefradil was also found to significantly speed up the inactivation kinetics of slower channels ($Ca_V1.2$, CEEE) with little effect on the inactivation kinetics of faster-inactivating channels ($Ca_V2.3$). A open-channel block model for mibefradil interaction with high-voltage-activated Ca^{2+} channels is discussed and shown to qualitatively account for our observations. Hence, our data agree reasonably well with a "receptor guarded mechanism" where fast inactivation kinetics efficiently trap mibefradil into the channel.

Key words: *Xenopus* oocytes — Receptor-modulated hypothesis — Site-directed mutagenesis — Calcium — Inactivation — Use-dependent block

Introduction

It has been well established that clinically important drugs, including local anesthetics, some anticonvulsants and antiarrhythmics, exert their therapeutic effects by preferentially altering the inactivated state of voltage-dependent K^+, Na^+, and Ca^{2+} channels (Hille, 1992). Frequency-dependent inhibition is central to their action, as drugs become most highly effective when channels are repetitively stimulated. State-dependent inhibition was first characterized on Na^+ channels (Hille, 1977) and is usually inferred from key biophysical properties including voltage-dependence of channel inhibition, use-dependent inhibition, and drug-induced changes in channel gating (Hering et al., 1998; Yarov-Yarovoy et al., 2001).

Mibefradil (RO 40-5967) is a Ca^{2+}-channel antago-

Correspondence to: L. Parent; email: lucie.parent@umontreal.ca

nist that has been used clinically as an anti-hypertensive and antianginal agent (Clozel, Banken & Osterrieder, 1989; Clozel, Ertel & Ertel, 1997). Sold commercially for some years under the brand name Posicor, mibefradil was later withdrawn by Hoffmann-LaRoche because it was shown to interfere with cytochrome P450 in the liver. The nondihydropyridine calcium blocker exerts a potent inhibitory effect on T-type Ca^{2+} currents in vascular smooth muscle cells (Mishra & Hermsmeyer, 1994), sensory neurons (Todorovic & Lingle, 1998), spermatogenic cells (Arnoult, Villaz & Florman, 1998), and adrenal cortisol-secreting cells (Esneu, Gallo-Payet & Payet, 1998; Gomora et al., 2000) as well as on recombinant T-type channels (Klugbauer et al., 1999; Williams et al., 1999; Lacinova, Klugbauer & Hofmann, 2000a; Martin et al., 2000; McNaughton et al., 2000; Monteil et al., 2000; Perchenet, Benardeau & Ertel, 2000a). Nonetheless, mibefradil is also known to block non-T-type calcium currents such as native L-type calcium currents in rabbit sinus node cells (Protas & Robinson, 2000), in myoblasts (Liu et al., 1999) and in pancreatic β-cells (Wu et al., 2000) as well as in recombinant $Ca_V1.2$, $Ca_V2.1$, $Ca_V2.2$, and $Ca_V2.3$ channels (Bezprozvanny & Tsien, 1995; Aczel, Kurka & Hering, 1998; Jimenez et al., 2000). Recently, it was reported that mibefradil could also inhibit with high affinity (μM range) the voltage-dependent K^+ channel hKv1.5 with a *Kd* of 0.8 μM (Perchenet & Clement-Chomienne, 2000b), HERG and KvLQT1 channels (Chouabe et al., 1998), and voltage-dependent Na^+ channels (Eller et al., 2000). It remains to be seen whether a unique molecular motif underlies the interaction of mibefradil with all these structurally divergent channels.

Studies aimed at determining the mechanisms of inhibition of voltage-dependent recombinant calcium channels by mibefradil have yet to identify the molecular determinants of mibefradil binding to the channels. The observation that mibefradil appears to compete with Ba^{2+} and Ca^{2+} ions could suggest that it interacts directly with the pore region (Martin et al., 2000). An overwhelming majority of the studies has demonstrated some voltage- and use-dependent block by mibefradil (Bezprozvanny & Tsien, 1995; Jimenez et al., 2000; Lacinova et al., 2000a) on Ca^{2+} channels. Voltage-dependent block by mibefradil was reported for expressed $Ca_V1.2$ channels, either the cardiac α1C-a (Bezprozvanny & Tsien, 1995; Lacinova et al., 1995), the smooth muscle α1C-b (Welling et al., 1995), or the brain α1C-c (Jimenez et al., 2000), and for $Ca_V2.3$ (Bezprozvanny & Tsien, 1995; Jimenez et al., 2000). In terms of the modulated receptor hypothesis (Hille, 1977), the higher efficiency of mibefradil at depolarized voltages was interpreted as predominant drug binding to inactivated channels. Nonetheless, the molecular mechanism of mibefradil interaction with closed, open, and inactivated channels is still controversial. For $Ca_V1.2$, $Ca_V2.1$, $Ca_V2.2$, and $Ca_V2.3$ channels expressed in *Xenopus* oocytes, open channel block by mibefradil was indicated by drug-induced acceleration of the inactivation kinetics (Bezprozvanny & Tsien, 1995). This conclusion was apparently contradicted by a recent study showing that the rate of inactivation in chimeric $Ca_V1.2/Ca_V2.1$ channels does not correlate with mibefradil block (Aczel et al., 1998). The problem might be compounded by the observation that mibefradil could accumulate inside mammalian cells as the des-methoxyacetyl mibefradil metabolite (Wu et al., 2000).

To investigate the state-dependent inhibition by mibefradil, we analyzed the inhibition of wild-type and inactivation-altered $Ca_V1.2$ and $Ca_V2.3$ channels (Bernatchez et al., 2001; Berrou et al., 2001). The inactivation kinetics of high-voltage-activated Ca^{2+} channels were recently shown to be significantly altered by point mutations in the I–II linker (Bourinet et al., 1999; Cens et al., 1999; Berrou et al., 2001; Parent et al., 2001). As we have recently shown, point mutations in the I–II linker of $Ca_V2.3$ channels, and more specifically in the nonconserved residues of the β-subunit binding motif, disrupted the kinetics and voltage-dependence of inactivation, whereas reverse mutations in $Ca_V1.2$ accelerated inactivation kinetics (Berrou et al., 2001; Parent et al., 2001). In particular, the EC(*AID*)EEE chimera, with the β-subunit binding domain from $Ca_V1.2$ was faster than CEEE, whereas EC(*IS1-6*)EEE was not significantly different from $Ca_V2.3$ (Bernatchez et al., 2001; Parent et al., 2001). Using these mutants we showed that mibefradil inhibition increased with faster inactivation kinetics. Dose-response curves were superimposable for the faster EC(*IS1-6*)EEE and $Ca_V2.3$ channels with $IC_{50} \approx 7–9$ μM. The channels with intermediate inactivation kinetics (CEEE, $Ca_V1.2$ E462R, and $Ca_V1.2$ E462K) were inhibited by intermediate concentrations of mibefradil with $IC_{50} \approx 55–75$ μM, whereas the slower $Ca_V1.2$ wild-type and $Ca_V1.2$ Q473K channels responded to higher doses of mibefradil with $IC_{50} \approx 100–120$ μM. Significant differences were also observed in terms of mibefradil modulating the channel's inactivation kinetics. Mibefradil significantly sped up the inactivation kinetics of slower channels with little effect on the inactivation kinetics of faster-inactivating channels. Altogether, our data are compatible with a simple kinetic model where mibefradil binding to the channel-open state restricts transitions back to the closed state.

Materials and Methods

Recombinant DNA Techniques

Standard methods of plasmid DNA preparation were used (Sambrook, Fritsch & Maniatis, 1989). cDNAs coding for wild-type rabbit $Ca_V1.2$

(α1C or C) (GenBank X15539) and β3 (Genbank M88751) were kindly donated by Dr. E. Perez-Reyes. The wild-type human $Ca_V2.3$ (α1E or E) (GenBank L27745) was a gift from Dr. T. Schneider. The rat brain α2bδ subunit was provided by Dr. T.P. Snutch. The construction of the C/E chimeras was described elsewhere (Bernatchez et al., 2001). Briefly, the chimera CEEE was constructed by transposing the region included between 87–510 AA from C into E, which corresponds roughly to Repeat I plus part of the I-II linker; EC(*AID*)EEE was obtained by introducing the 425–510 AA region from C into E and corresponds roughly to the β-subunit binding motif in the I-II linker; EC(*IS1-6*)EEE was obtained by swapping the transmembrane segments from Repeat I (87–425 AA) of C into E. The construction of point mutations $Ca_V1.2$ E462R, $Ca_V1.2$ E462K, $Ca_V1.2$ Q473K, and $Ca_V2.3$ R378E has been described earlier (Berrou et al., 2001). cDNA constructs were linearized at the 3′ end and run-off transcripts were prepared using methylated cap analog $m^7G(5')ppp(5')G$ and T7 RNA polymerase with the mMessage mMachine® transcription kit (Ambion, Austin, TX). The final cRNA products were resuspended in DEPC-treated H_2O and stored at −80°C.

Functional Expression of Wild-type and Mutant Channels

Female *Xenopus* laevis clawed toad (Nasco, Fort Atkinson, WI) were anesthetized by immersion in 0.1% tricaine or MS-222 (3-aminobenzoic acid ethyl ester; Sigma, St. Louis, MO) for 15 minutes before surgery, as detailed before (Parent & Gopalakrishnan, 1995a; Parent et al., 1997; Bernatchez, Talwar & Parent, 1998). Stage V and VI oocytes were injected with cRNA coding for the α1 subunits (chimeras, mutants, and wild-type) along with cRNA coding for rat brain α2bδ (Williams et al., 1992), and the rat brain β3 (Castellano et al., 1993). Oocytes were incubated at 19°C in a Barth's solution for 3–5 days before experiments.

Solutions

Mibefradil was dissolved in H_2O and stored for one week at −20°C as either 1 M, 100 mM, 10 mM, or 1 mM stock solutions. Aliquots of the stock solutions were freshly diluted in the bath solutions at the indicated concentrations and used within the same day. Bath solutions were perfused at a rate of 1 ml/min and complete bath exchange was achieved within 30 sec. Tonic inhibition was recorded 1 minute after the perfusion of the drug.

Electrophysiological Recordings in Oocytes

Whole-cell currents were recorded at room temperature using a two-electrode voltage-clamp amplifier (OC-725C, Warner Instruments, Hamden, CT) as described earlier (Parent et al., 1995b; Parent et al., 1997; Bernatchez et al., 1998). Unless stated otherwise, currents were measured with a "10 Ba^{2+}" solution (in mM: 10 $Ba(OH)_2$; 110 NaOH; 1 KOH; 20 HEPES titrated to pH 7.3 with methane sulfonic acid (MeS)). To minimize endogenous Ca^{2+}-activated Cl^- currents, oocytes were injected with 18.4 nl of a 50 mM EGTA (ethylene glycol-bis(b-aminoethyl ether)-N,N,N′,N′-tetraacetic acid) (Sigma, St. Louis, MO) 1 to 2 hours before the experiments. Capacitive transients were erased for clarity in the final figures.

Data Acquisition and Analysis

PClamp software (Axon Instruments, Foster City, CA) was used for online data acquisition and analysis. Data were sampled at 10 kHz and low-pass filtered at 5 kHz, using the amplifier built-in filter. Unless indicated otherwise, whole-cell currents were elicited from a holding potential of −80 mV and measured using 450-msec voltage pulses from −40 to +60 mV at a frequency of 0.2 Hz (1 pulse every 5 sec) to minimize channel accumulation in the inactivated state. Current traces were corrected for linear leak and cell capacitance. Tonic inhibition was reported as the ratio of peak I_{Ba} at any given mibefradil concentration versus peak I_{Ba} at 0 μM. Dose-response data points were fitted to a simple one-site inhibition curve using Origin 6.1. Use-dependent block was measured in the presence of half-inhibitory concentrations of mibefradil (either 100 μM or 10 μM) using 50-msec depolarizing pulses applied from holding potential (HP) = −80 mV ($Ca_V1.2$) or −100 mV ($Ca_V2.3$). Currents were measured at the peak voltage at frequencies varying from 0.2 to 4 Hz ($Ca_V1.2$) or between 0.2 to 1 Hz ($Ca_V2.3$). No significant cumulative inactivation was observed under these conditions for the expressed channels in the absence of mibefradil.

Isochronal inactivation data (pseudo *h inf*) were measured at the test pulse of 0 mV after a series of 5-sec prepulses applied from −100 to +30 mV (Parent et al., 1995b).

$$\frac{i}{i_{max}} = 1 - \frac{1 - Y_0}{1 + \left\{\exp - \frac{zF}{RT}(V_m - E_{0.5})\right\}} \quad (1)$$

Pooled data (mean ± SEM) were fitted to the Boltzmann equation 1, which accounts for the fraction of non-inactivating current with $E_{0.5}$, mid-point potential; z, slope parameter; Y_0, fraction of non-inactivating current; V_m, the prepulse potential, and RT/F with their usual meanings.

Recovery from voltage-dependent inactivation was measured using mid-inhibitory concentrations of either 10 μM ($Ca_V2.3$) or 100 μM ($Ca_V1.2$). Inactivation was produced by a 5-sec pulse to 0 mV and channels were allowed to recover from inactivation for a variable duration (20 msec to 2.5 sec) from a holding potential of −80 mV. Peak currents measured during the test pulse were normalized to the peak current measured during the control pulse. Relative currents (Y) were fitted to equation 2 using Clampfit fitting routines.

$$Y = Y_0 + A_1\left(1 - \exp\left(\frac{-t}{\tau_1}\right)\right) + A_2\left(1 - \exp\left(\frac{-t}{\tau_2}\right)\right), \quad (2)$$

where A_1 and A_2 account for the respective contribution of each exponential function to the recovery process. Inactivation kinetics were quantified using *r300* values or the ratio of the whole-cell current remaining at the end of a 300-ms pulse (Peterson et al., 2000; Berrou et al., 2001).

Statistics

Results are presented as mean ± SEM. Independent Students's *t*-test was used for statistical comparison in Figs. 1–5. Paired Student's *t*-test was used to determine the significance of inactivation data reported before and after the addition of mibefradil on Figures 6–7.

Results

Voltage-dependent Inhibition of $Ca_V1.2$ and $Ca_V2.3$ Channels by Mibefradil

$Ca_V1.2$ (α1C) and $Ca_V2.3$ (α1E) were expressed in *Xenopus* oocytes in the presence of α2bδ and β3 subunits. Mibefradil inhibited whole-cell currents of both channels in a dose-dependent manner between 0.1 μM to 1 mM. Figure 1*A–D* shows typical whole-cell traces obtained in the presence of 10 mM Ba^{2+} for $Ca_V1.2$ (*A*) and

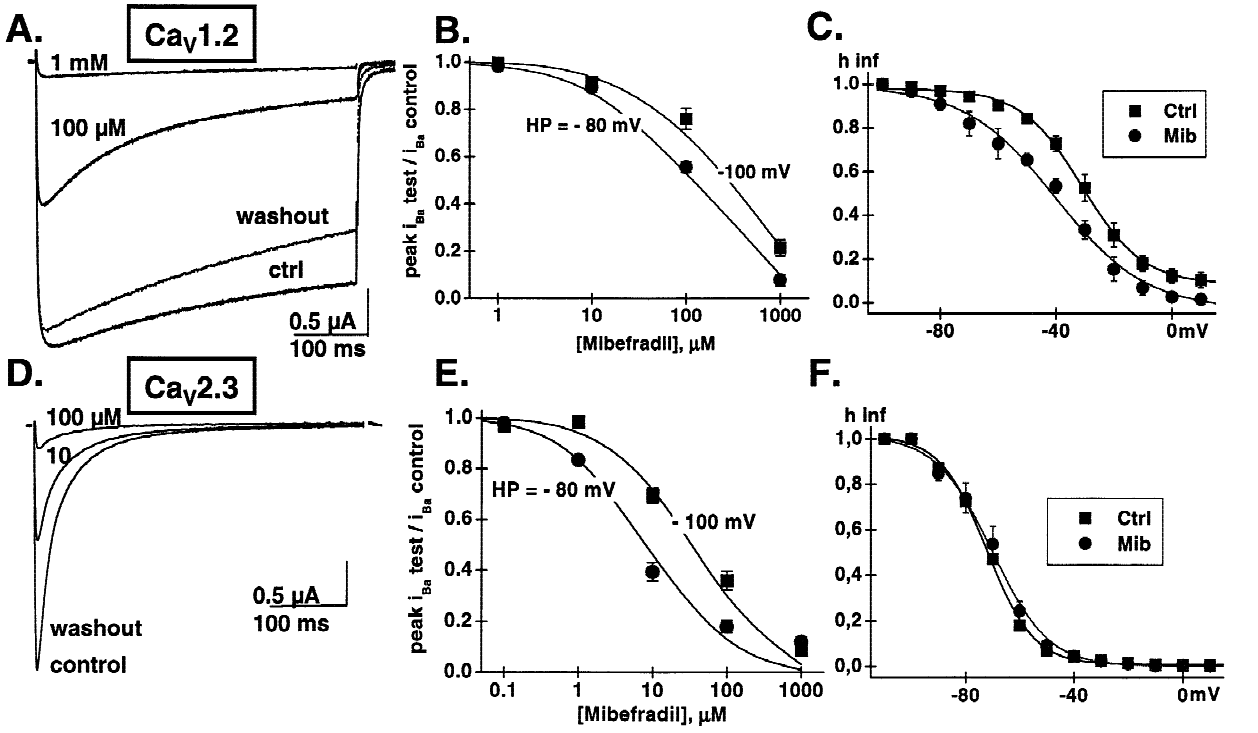

Fig. 1. Dose-dependent inhibition of $Ca_V1.2$ and $Ca_V2.3$ channels is voltage-dependent. $Ca_V1.2$ and $Ca_V2.3$ were expressed in *Xenopus* oocytes with $\alpha 2b\delta$ and $\beta 3$ subunits. (*A–C*) $Ca_V1.2$ data. (*A*) Typical whole-cell current traces recorded in 10 mM Ba^{2+} at 0 mV from a holding potential of −80 mV are shown for $Ca_V1.2$ in the presence of 0, 100 µM, and 1 mM mibefradil. The thin trace shows that the peak current was mostly restored upon the drug washout. (*B*) Dose-response curve was shifted to the right with holding potential (*HP*) = −100 mV. The mid-inhibitory concentration required to inhibit $Ca_V1.2$ channels increased from IC_{50} = 108 ± 21 µM (n = 7) at *HP* = −80 mV to 288 ± 17 µM (n = 3) at *HP* = −100 mV. (*C*) Mibefradil shifted the voltage-dependence of inactivation in $Ca_V1.2$ channels. Voltage-dependence of inactivation was measured at the end of 5 sec-prepulses and relative currents were fitted to the Boltzmann equation (1). The addition of 100 µM mibefradil shifted the inactivation curve from $E_{0.5}$ = −31 ± 3 mV and z = 2.5 ± 0.3 (n = 11) to $E_{0.5}$ = −43 ± 3 mV and z = 1.5 ± 0.4 (n = 4). (*D–F*) $Ca_V2.3$ data. (*D*) Typical $Ca_V2.3$ traces recorded at 0 mV (*HP* = −80 mV) in the presence of 0, 10 and 100 µM mibefradil. The thin trace peak current after drug washout is indistinguishable from the control currents. (*E*) Dose-response curve was shifted to the right with an increase in holding potential. The mid-inhibitory concentration required to inhibit $Ca_V2.3$ increased from IC_{50} = 8 ± 2 µM (n = 9) at *HP* = −80 mV to 33 ± 7 µM (n = 4) at *HP* = −100 mV. (*F*) Mibefradil (10 µM) did not affect the voltage-dependence of inactivation in $Ca_V2.3$ channels: $E_{0.5}$ = −72 ± 4 mV and z = 2.7 ± 0.3 (n = 4) without mibefradil; $E_{0.5}$ = −73 ± 3 mV and z = 2.7 ± 0.4 (n = 3) with mibefradil. Data are reported as mean ± SEM.

$Ca_V2.3$ (*D*) at increasing concentrations of mibefradil from a holding potential of −80 mV. Drug washout is shown as the thin trace. For $Ca_V2.3$, the whole-cell current measured after washout current was identical to the control value. Under these conditions, $Ca_V1.2$ appears to be 10-fold less sensitive to the extracellular application of mibefradil than $Ca_V2.3$. As seen, the addition of 10 µM mibefradil inhibited only 11 ± 2% (n = 7) of the $Ca_V1.2$ currents (*B*) as compared to a robust block of 61 ± 4% (n = 6) of the $Ca_V2.3$ currents (*E*) measured under similar conditions. The drug was clearly less effective (p < 0.001) on $Ca_V1.2$ than on $Ca_V2.3$ currents. Mibefradil inhibition was rapid (<1 minute) and peak currents were restored to >90% of the control currents within 20–25 minutes of the drug washout (Fig. 1 *A, D*). For $Ca_V1.2$, 92 ± 4% (n = 3) of the peak current inhibition was reversed after the washout period with the vehicle solution as compared to 97 ± 4% (n = 4) of the $Ca_V2.3$ whole-cell currents.

Dose-response curves were calculated from data collected at the peak voltage in the presence of 10 mM Ba^{2+} and fitted to a one-to-one inhibition equation (Fig. 1 *B, E*). Addition of mibefradil did not affect the peak current-voltage properties nor the channel's activation properties (*results not shown*). Depolarization between 0 and +20 mV increased the affinity of $Ca_V1.2$ channels from IC_{50} = 108 ± 21 µM to 64 ± 15 µM (n = 7), which suggests that mibefradil inhibition is state-dependent. In contrast, block of $Ca_V2.3$ channels was not significantly affected by test potentials between −10 and +30 mV. These data will be analyzed later in greater details (*see* Fig 7).

An increase in channel availability decreased mibefradil affinity for both channels (Fig. 1 *B, E*). As seen,

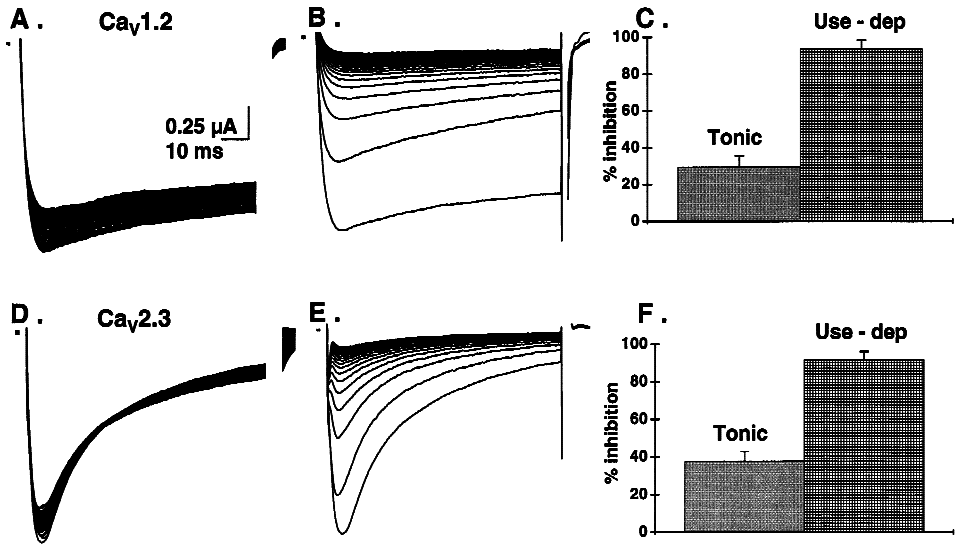

Fig. 2. Use-dependent inhibition of $Ca_V1.2$ and $Ca_V2.3$ channels. Frequency-dependent inhibition was measured using a series of 100-msec test pulses to 0 mV from a holding potential of −80 mV ($Ca_V1.2$) or −100 mV ($Ca_V2.3$). (*A*) $Ca_V1.2$ currents were measured under control conditions (no mibefradil) at a frequency of 1 Hz. (*B*) Addition of 100 μM mibefradil inhibited currents in a frequency-dependent manner. (*C*) Tonic inhibition (measured after the first pulse) was 38 ± 5% ($n = 4$) compared with 92 ± 4% ($n = 4$) at the end of the train of stimulations. (*D*) $Ca_V2.3$ currents were measured under control conditions (no mibefradil) at a frequency of 1 Hz. (*E*) Addition of 10 μM mibefradil inhibited currents in a frequency-dependent manner. (*F*) Tonic inhibition (measured after the first pulse) was 30 ± 6% ($n = 3$) as compared to 94 ± 5% ($n = 3$) at the end of the train of stimulations.

increasing the holding potential from −80 to −100 mV shifted the dose-response curve toward higher values. The mibefradil concentration required to inhibit half of the $Ca_V1.2$ currents (IC_{50}) doubled from a value of 108 ± 21 μM ($n = 7$) (HP = −80 mV) to 288 ± 17 μM ($n = 3$) ($HP = -100$ mV). In the presence of 10 μM mibefradil in the bath, peak Ba^{2+} inhibition was significantly different at $p < 0.01$ between −80 and −100 mV for $Ca_V1.2$. In contrast, the IC_{50} quadrupled from 8 ± 2 μM ($n = 9$) ($HP = -80$ mV) to 33 ± 7 μM ($n = 4$) ($HP = -100$ mV) for $Ca_V2.3$ ($p < 0.004$). The larger difference observed for $Ca_V2.3$ channels may be explained in part by a decreased channel availability at a holding potential of −80 mV coupled to the slower recovery from inactivation induced by mibefradil (*see later*).

Mibefradil slightly shifted the voltage-dependence of $Ca_V1.2$ inactivation toward more negative potentials from $E_{0.5} = -31 \pm 3$ mV ($n = 11$) to $E_{0.5} = -43 \pm 3$ mV ($n = 4$) ($p < 0.06$), when measured after 5-sec depolarizing pulses. The mibefradil-induced shift of ≈−10 mV in the inactivation of $Ca_V1.2$ was also accompanied by a decrease in the slope steepness. Under the same conditions, mibefradil did not significantly alter the voltage-dependence of $Ca_V2.3$ inactivation (Fig. 1 *C, F*).

Use-dependent Inhibition of $Ca_V1.2$ and $Ca_V2.3$ Channels by Mibefradil

In addition to voltage-dependent block, use-dependent inhibition was also reported for clinically relevant drugs such as calcium channel antagonists, local anesthetics and antiarrhythmics. Use-dependent blockers will preferentially inhibit ion channels during intense electrical activity. Use-dependent block is conditioned by repetitive opening of the channel and is enhanced upon increasing the stimulation frequency. Cumulative inhibition was obtained by firing a series of 50 test pulses to the peak voltage of 0 mV at either 1 Hz ($Ca_V2.3$) or 4 Hz ($Ca_V1.2$), using mid-inhibitory mibefradil concentrations (Fig. 2). Under control conditions, peak $Ca_V1.2$ currents remained relatively stable with ≈3 to 5% variations (Fig. 2 *A*). In contrast, we found that increasing the frequency of stimulation from 0.2 Hz to 1 Hz strongly decreased the peak current generated by $Ca_V2.3$ under the same conditions. This frequency-dependent rundown observed under control conditions probably reflects its slower kinetics of recovery from voltage-dependent inactivation (*see later*). At a pulse frequency of 1 Hz, $Ca_V1.2$ and $Ca_V2.3$ channels experienced significant use-dependent inhibition (Fig. 2 *B, E*). Mibefradil blocked 92 ± 4% ($n = 4$) as compared to tonic inhibition of 38 ± 5% ($n = 4$) of the $Ca_V1.2$ currents, whether stimulated at 1 or 4 Hz (Fig. 2 *C*). Note that $Ca_V1.2$ currents inactivated faster in the presence of mibefradil, as will be discussed later. Similarly, high-frequency stimulation (1 Hz) in the presence of mibefradil resulted in a 94 ± 5% ($n = 3$) decrease in $Ca_V2.3$ currents as compared to a tonic inhibition of 30 ± 6% ($n = 3$) (Fig. 2 *F*). Use-dependent inhibition confirms the interaction of mibefradil with either the open and/or the inactivated state of $Ca_V1.2$ and

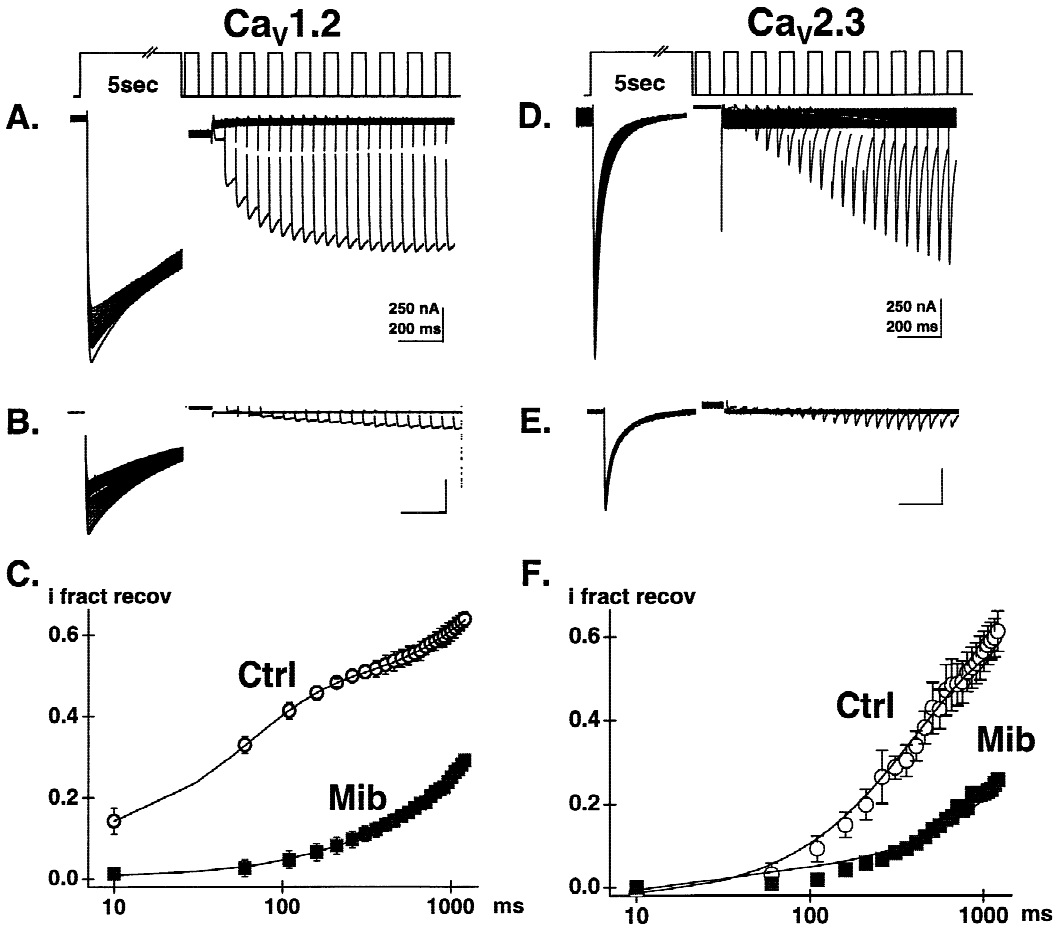

Fig. 3. Mibefradil slows I_{Ba} recovery from inactivation. Recovery from voltage-dependent inactivation was studied for $Ca_V1.2$ and $Ca_V2.3$ channels. The protocol used to examine recovery from inactivation is pictured with a break in the time scale between 1400 and 4800 msec. Inactivation was produced by a 5-sec pulse to 0 mV and channels were allowed to recover from inactivation for a variable duration (20 msec to 2.5 sec) from a holding potential of -8_0 mV. (*A*) Under control conditions, $Ca_V1.2$ recovery was described by a bi-exponential function with 37 ± 5% of the channels recovering with a fast $\tau_{rec\,(1)} = 61 \pm 15$ msec ($n = 5$). (*B*) After the addition of 100 μM mibefradil, fewer than 30% ($n = 3$) of the $Ca_V1.2$ channels had recovered at the end of a 1200-msec pulse compared with 64 ± 2% ($n = 5$) under control conditions. (*C*) The fractions of the peak $Ca_V1.2$ currents obtained under control conditions (open circles) and after the addition of mibefradil (filled squares) were plotted against a logarithmic time scale. Data were pooled and mean data ± SEM were fitted to the double-exponential equation 2 using the solver routine in Origin 6.1. (*D*) Under control conditions, $Ca_V2.3$ channels recovered more slowly than $Ca_V1.2$ with 41 ± 4% ($n = 6$) channels recovering with $\tau_{rec\,(1)} = 392 \pm 15$ msec ($n = 6$). (*E*) Addition of 10 μM mibefradil prevented normal $Ca_V2.3$ recovery. Only 26 ± 2% ($n = 3$) channels had recovered after a 1200-msec pulse to −80 mV compared with 61 ± 5% ($n = 6$) under control conditions. (*F*) The fractions of the peak $Ca_V2.3$ currents obtained under control conditions (open circles) and after the addition of mibefradil (filled squares) were plotted against a logarithmic time scale. The lines connecting the data points were obtained from the best fits to equation 2.

$Ca_V2.3$ channels, but does not permit to distinguish either situation, a conclusion also reached for $Ca_V2.1$ (Jimenez et al., 2000).

Mibefradil Impaired I_{Ba} Recovery from Inactivation

Experiments were designed to characterize the effect of mibefradil on the kinetics of recovery from voltage-dependent inactivation using mid-inhibitory mibefradil concentrations of 10 μM ($Ca_V2.3$) or 100 μM ($Ca_V1.2$). Inactivation was produced by 5-sec pulses to the peak voltage and channels were allowed to recover from inactivation for a variable duration (20 msec to 2.5 sec) from a holding potential of −80 mV, using the protocol shown in Fig. 3. In the absence of mibefradil, $Ca_V1.2$ recovery was well described by a bi-exponential function with 37 ± 3% of the channels recovering with a fast $\tau_{rec\,(1)} = 61 \pm 7$ msec ($n = 5$) (Table), suggesting the presence of two kinetically distinct inactivated states in $Ca_V1.2$ (Fig. 3 *A–C*). In contrast, $Ca_V2.3$-channel activity recovered more gradually with 50 ± 6% ($n = 6$) of the channels being recovered with $\tau_{rec\,(1)} = 395 \pm 33$

Table. Recovery from voltage-dependent inactivation for $Ca_V2.3$ and $Ca_V1.2$ wt and mutants

+ α2bδ/β3	Mib μM	A_1	τ_1 msec	A_2	τ_2 msec
$Ca_V2.3$ wt	0	0.50 ± 0.06	395 ± 33	0.4 ± 0.1	1985 ± 346
	10	0.41 ± 0.03	1053 ± 315	0.3 ± 0.2	9543 ± 1256
$Ca_V2.3$ R378E	0	0.21 ± 0.04	213 ± 17	0.72 ± 0.08	2536 ± 162
	10	0.13 ± 0.06	598 ± 122	0.7 ± 0.1	6137 ± 1420
EC(*AID*)EEE	0	0.49 ± 0.04	83 ± 3	0.45 ± 0.07	3720 ± 210
	10	0.19 ± 0.05	173 ± 10	0.80 ± 0.08	8710 ± 2505
CEEE	0	0.45 ± 0.03	115 ± 33	0.38 ± 0.08	2150 ± 476
	100	0.21 ± 0.02	175 ± 21	0.57 ± 0.09	9567 ± 2134
$Ca_V1.2$ E462R	0	0.45 ± 0.04	65 ± 3	0.55 ± 0.06	2074 ± 63
	100	0.14 ± 0.03	143 ± 45	0.86 ± 0.04	2610 ± 1153
$Ca_V1.2$ wt	0	0.37 ± 0.03	61 ± 7	0.54 ± 0.05	2750 ± 236
	100	0.11 ± 0.05	610 ± 114	0.72 ± 0.07	9682 ± 2356

Recovery from inactivation for $Ca_V2.3$ wt, $Ca_V2.3$ R378E, EC(*AID*)EEE, CEEE, $Ca_V1.2$ E462R, and $Ca_V1.2$ wt channels expressed in *Xenopus* oocytes with α2bδ and β3 subunits and recorded in 10 mM Ba^{2+} in the absence and in the presence of the mid-inhibitory concentrations of mibefradil as indicated. Inactivation was produced by a 5 sec pulse to 0 mV and channels were allowed to recover from inactivation for a variable duration (20 msec to 2.5 sec) from a holding potential of −80 mV. The time constants of the recovery from inactivation and their relative amplitudes were obtained after fitting the mean data averaging 3–6 individual experiments. Data were fitted to the double-exponential equation 2 (*see* Materials and Methods). Fits ± standard errors are provided.

msec ($n = 6$) (Fig. 3 *D–F*) (Table). The $Ca_V2.3$ recovery was also found to significantly improve from a holding potential of −120 mV, unlike $Ca_V1.2$ recovery (*results not shown*). Although their time course varied quite significantly, a 2-sec pulse to −80 mV succeeded in recovering about 95% of $Ca_V1.2$ and 70% of $Ca_V2.3$ currents. The slower recovery of $Ca_V2.3$ channels under control conditions is likely to lock channels in the inactivated state, which could explain why use-dependent block by mibefradil could never be documented at a frequency higher than 1 Hz.

Mibefradil introduced a significant 100-msec lag in channel recovery, yielding a drastically altered time course with less than 5% of either channel's recovery at 120 msec. In particular, mibefradil completely eradicated the fast-recovery time constant that was present in $Ca_V1.2$ channels. Only 29 ± 1% ($n = 3$) of the $Ca_V1.2$ currents recovered in the presence of 100 μM mibefradil in contrast to 64 ± 2% ($n = 5$) under control conditions. In the presence of 10 μM mibefradil, $Ca_V2.3$ recovery was decreased from 61 ± 5% ($n = 6$) to 26 ± 2% ($n = 3$) after a 1200-msec pulse to −80 mV. Similarly, a drug-induced delay in the onset of recovery from inactivation has also been reported for the inhibition of recombinant $Ca_V1.2$ channels by dihydropyridines and phenylalkylamines (Hering et al., 1997; Lacinova, Klugbauer & Hofmann, 2000b). This observation strongly suggests that the drug is locking channels in an absorbing inactivated state.

Dose-dependent Inhibition of Inactivation-modified $Ca_V1.2$ and $Ca_V2.3$ Channels

To address the role of inactivation, we performed a series of experiments with $Ca_V1.2$ and $Ca_V2.3$ chimeras and mutants with altered inactivation kinetics. As we have previously shown, point mutations and chimeras in the I-II linker of $Ca_V2.3$ channels, and more specifically in the nonconserved residues of the β-subunit binding motif, could significantly decrease inactivation kinetics and voltage-dependence, whereas reverse mutations in $Ca_V1.2$ accelerated inactivation kinetics (Berrou et al., 2001; Parent et al., 2001). The CEEE chimera (Repeat I + part of the I-II linker from $Ca_V1.2$) displayed voltage-dependent inactivation properties similar to $Ca_V1.2$ despite being more than 90% homologous to $Ca_V2.3$. The smaller chimera EC(*AID*)EEE, with the β-subunit binding domain from $Ca_V1.2$ was slightly faster than CEEE whereas EC(*IS1-6*)EEE was not significantly different from $Ca_V2.3$ (Parent et al., 2001). Although mutations were performed within and around the β-subunit binding site, the mutant channels retained their modulation by β-subunits. The inactivation state in these mutant channels was found to be specifically targeted, as activation properties were not significantly affected.

Figure 4 *A–E* shows typical current traces obtained at the peak voltage (either −10 or 0 mV) in the presence of 10 mM Ba^{2+} from a holding potential of −80 mV at three mibefradil concentrations (0.1 μM, 10 μM, and 1 mM). Peak current-voltage relationships were not affected by the addition of mibefradil to the bath, and peak currents were restored readily upon the drug washout. Mibefradil inhibition was significantly enhanced in faster inactivating channels, whereas it was significantly reduced in slower channels. In the presence of 10 μM mibefradil, 64 ± 3% ($n = 4$) of EC(*IS1-6*)EEE and 60 ± 2% ($n = 5$) of $Ca_V2.3$ whole-cell currents were inhibited in contrast to 11 ± 5% ($n = 6$) for $Ca_V1.2$, 16 ± 2% ($n = 4$) for CEEE, 18 ± 4% ($n = 4$) for $Ca_V1.2$ E462R, and

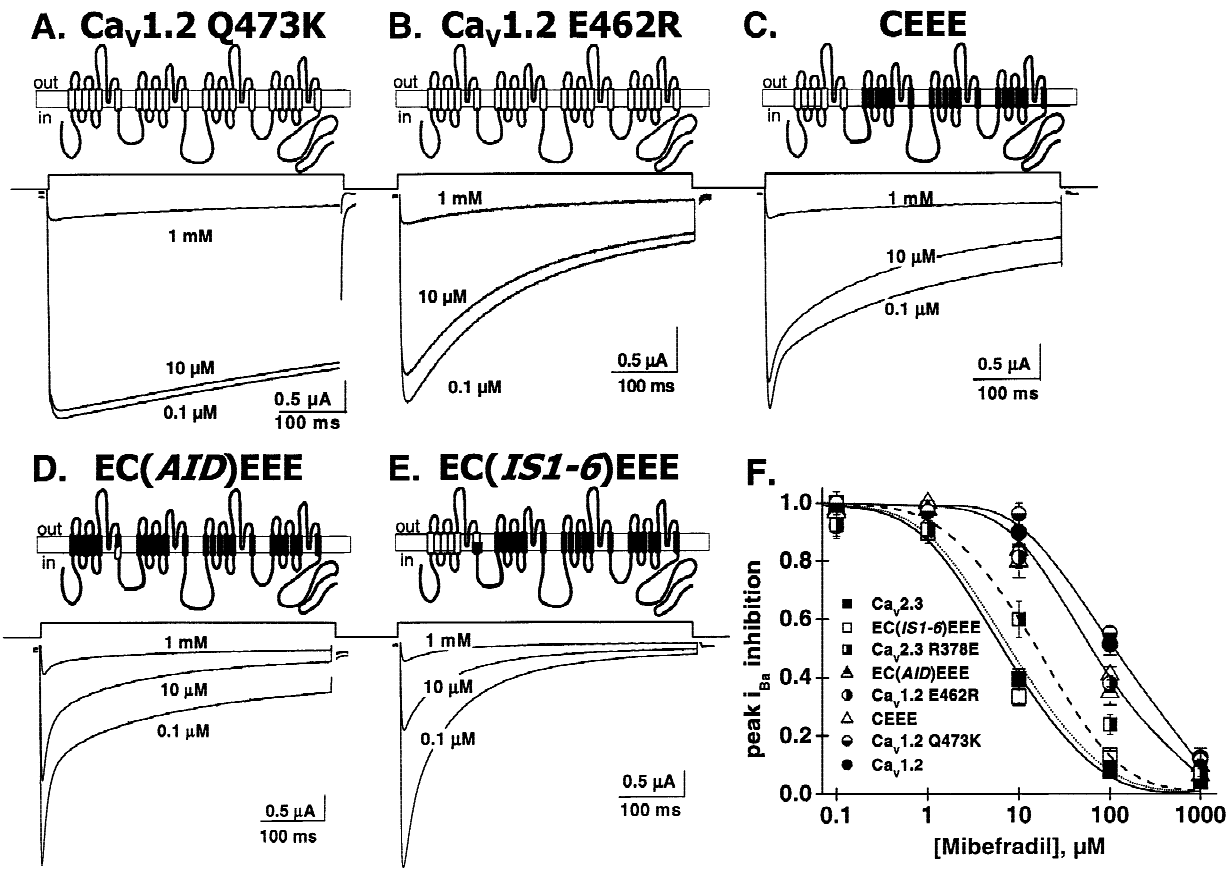

Fig. 4. Dose-dependent inhibition of $Ca_V1.2$ and $Ca_V2.3$ mutant channels. $Ca_V1.2$ and $Ca_V2.3$ mutants were expressed in *Xenopus* oocytes with $\alpha 2b\delta$ and $\beta 3$ subunits. Typical whole-cell current traces recorded in 10 mM Ba^{2+} at 0 mV from a holding potential of −80 mV are shown after the addition of 0.1 µM, 10 µM, and 1 mM mibefradil. (*A*) The Q473K mutation in $Ca_V1.2$ switched a nonconserved residue from $Ca_V1.2$ to $Ca_V2.3$ in the *AID* binding site in the I-II linker with little effect on whole-cell inactivation kinetics. (*B*) The E462R mutation in $Ca_V1.2$ significantly sped up inactivation kinetics. (*C–D*) The CEEE and EC(*AID*)EEE chimeras displayed inactivation kinetics significantly slower than the wild-type $Ca_V2.3$. (*E*) The EC(*IS1-6*)EEE chimera inactivated like the wild-type $Ca_V2.3$ channel. (*F*) Dose-response curves are shown superimposed for wild-type and mutant channels. The number of independent experiments was $n = 3$–9 for each channel. The lines connecting the data points were obtained from the best fits of the pooled data for each channel to a one-to-one binding equation. The calculated IC_{50} values were 8 ± 2 µM ($n = 9$) for $Ca_V2.3$; 7 ± 1 µM ($n = 3$) for EC(*IS1-6*)EEE; 31 ± 4 µM ($n = 5$) for $Ca_V2.3$ R378E; 41 ± 5 µM ($n = 4$) for EC(*AID*)EEE; 58 ± 7 µM ($n = 6$) for $Ca_V1.2$ E462R; 68 ± 9 µM ($n = 5$) for CEEE; 117 ± 12 µM ($n = 3$) for $Ca_V1.2$ Q473K; 108 ± 21 µM ($n = 7$) for $Ca_V1.2$.

28 ± 7% ($n = 4$) for EC(*AID*)EEE. Mibefradil inhibition was significantly different at $p < 0.001$ for CEEE and EC(*IS1-6*)EEE chimeras, despite their closely-related primary structures (>97% identity). The dose-response curves, calculated from the averaged data points, were superimposable for faster EC(*IS1-6*)EEE and $Ca_V2.3$ and were indistinguishable for slower Q473K and wild-type $Ca_V1.2$ channels (Fig. 4 *F*).

As seen with the wild-type channels, mibefradil significantly delayed channel recovery from inactivation in inactivation-deficient CEEE, EC(*AID*)EEE, $Ca_V1.2$ E462R, and $Ca_V2.3$ R378E channels (Fig. 5). In the absence of mibefradil, the time course of channel recovery for CEEE, EC(*AID*)EEE, and $Ca_V1.2$ E462R channels was reminiscent of $Ca_V1.2$, suggesting that mutations in the I-II linker affected in a similar fashion both transition to the inactivated state and its recovery. Mutant $Ca_V2.3$ R378E behaved like its parent $Ca_V2.3$ (*see* Fig. 3) with a slower recovery than other mutants. Again, mibefradil introduced a significant 100 msec-lag in channel reprimming, which was more prominent for $Ca_V2.3$ R378E but remained noticeable for all channels. In the presence of mid-inhibitory concentrations of mibefradil, 60 to 75% of the channels remained locked in the inactivated state at the end of a 1200 msec pulse to −80 mV as compared to 30 to 50% in the absence of the drug.

Drug-induced Changes in Inactivation Gating

The inactivation kinetics of $Ca_V1.2$ and $Ca_V2.3$ mutants were reported before and after the addition of mid-

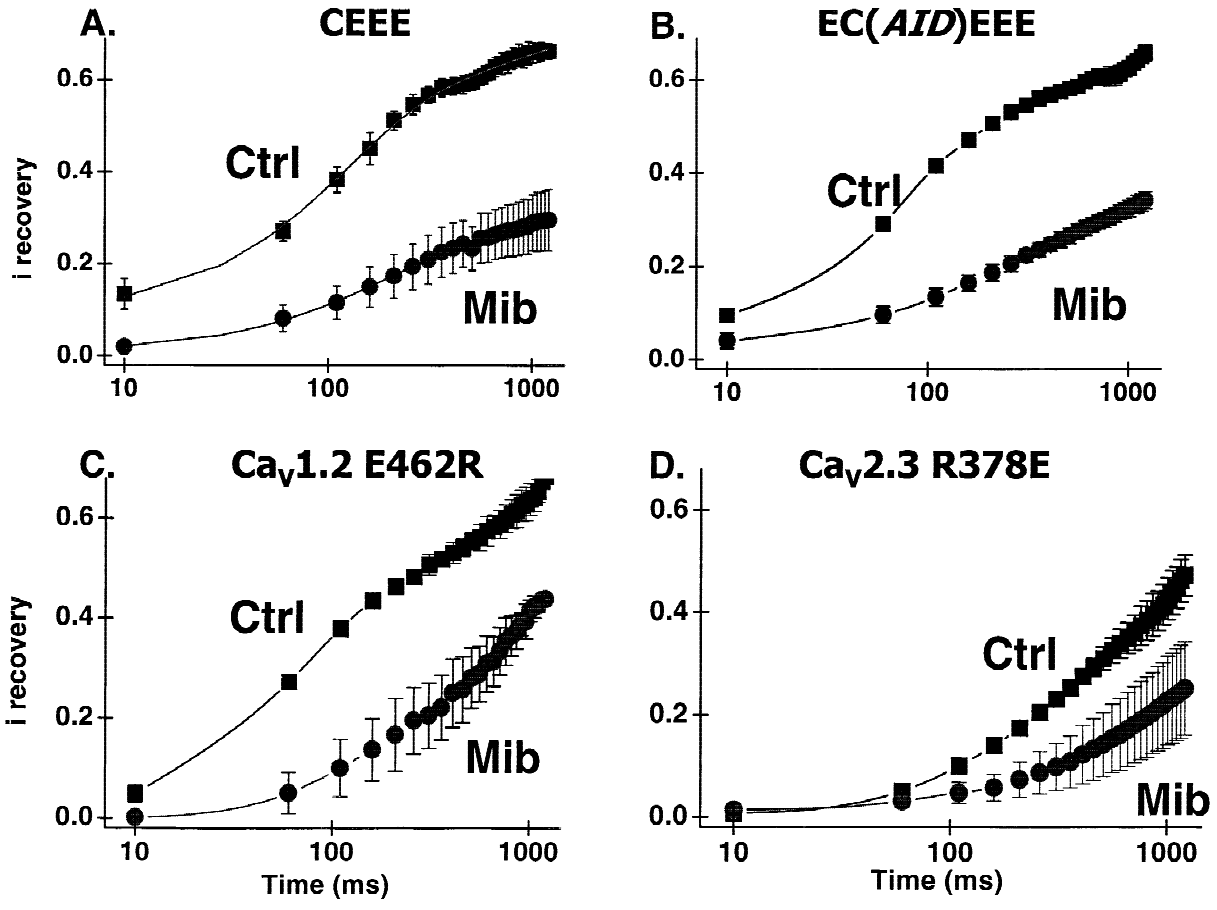

Fig. 5. Mibefradil slows I_{Ba} recovery for inactivation-deficient channels. Recovery from voltage-dependent inactivation was analyzed in the presence of 10 μM mibefradil (EC(*AID*)EEE and $Ca_V2.3$ R378E) or 100 μM mibefradil (CEEE and $Ca_V1.2$ E462R). The protocol used was shown in Fig. 3. The fractions of the peak currents obtained under control conditions (filled squares) and after the addition of mibefradil (gray circles) were plotted against a logarithmic time scale. Data were pooled and mean data ± SEM were fitted to a double-exponential equation using the solver routine in Origin 6.1. (*A–C*) CEEE, EC(*AID*)EEE, and $Ca_V1.2$ E462R recovered from inactivation following a time course similar to $Ca_V1.2$ under control conditions with a relatively fast onset with $\tau_1 < 100$ msec. (*D*) Both in the absence and in the presence of mibefradil, $Ca_V2.3$ R378E displayed the slow onset of recovery that is typical of $Ca_V2.3$. The lines connecting the data points were obtained from the best fits to equation 2. Fit values are shown in the Table.

inhibitory concentrations of mibefradil in the bath in the presence of the vehicle solution (10 Ba^{2+}). The *r300* values reported for the wild-type and mutant channels are comparable to values previously reported, thus supporting the role of the I-II linker in the voltage-dependent inactivation gating of $Ca_V2.3$ (Berrou et al., 2001). As shown in Fig. 6, mibefradil significantly accelerated the inactivation kinetics of $Ca_V1.2$ at −10 mV ($p < 0.0005$). Depolarization from −10 to +20 mV further enhanced the effect of mibefradil on inactivation kinetics. Drug-induced increase in inactivation kinetics was also observed to a smaller extent with the CEEE chimera and with $Ca_V1.2$ E462R ($p < 0.02$). In contrast, the effects of mibefradil on the inactivation kinetics of wild-type $Ca_V2.3$ as well as on mutant $Ca_V2.3$ R378E, chimeras EC(*AID*)EEE and EC(*IS1-6*)EEE, were not significant ($p < 0.1$), even at +10 and +20 mV. In this regard, mibefradil accelerated the inactivation kinetics of slower inactivating channels, whereas it seemingly failed to significantly affect the kinetics of fast-inactivating channels.

Voltage-induced Changes in Mibefradil Affinity

The influence of membrane potential on mibefradil affinity was investigated between 0 and +20 mV. As seen in Fig. 7, depolarization significantly increased the affinity of $Ca_V1.2$ channels for mibefradil, as IC_{50} decreased from 108 ± 21 μM at 0 mV to 64 ± 15 μM at +20 mV ($n = 7$). Addition of 10 μM mibefradil inhibited 26 ± 3% of the $Ca_V1.2$ whole-cell currents measured at +20 mV as compared to only 10 ± 4% at 0 mV ($p < 0.01$). Depolarization also significantly increased mibefradil af-

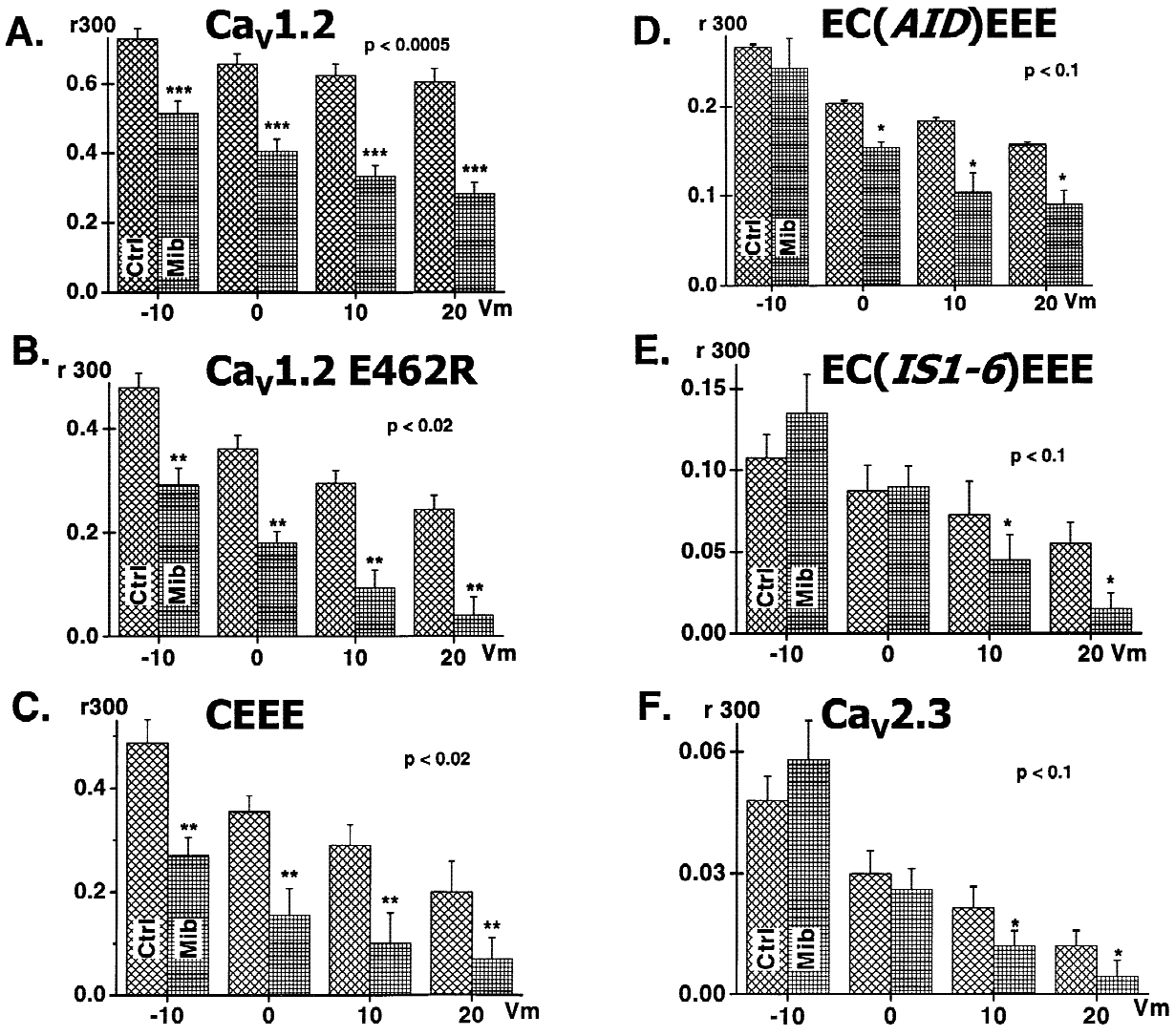

Fig. 6. Mibefradil accelerated inactivation kinetics of $Ca_V1.2$. The inactivation kinetics of $Ca_V1.2$ and $Ca_V2.3$ mutants are shown before and after the addition of mid-inhibitory concentrations of mibefradil as a function of the membrane potential. Inactivation kinetics were quantified by evaluating the ratio of the whole-cell current remaining at the end of a 300-msec pulse (*r300*). Paired measurements were made in 4–9 experiments. (*A–C*) Mibefradil (100 μM) significantly accelerated the inactivation kinetics between −10 mV and +20 mV of $Ca_V1.2$ ($p < 0.0005$), $Ca_V1.2$ E462R ($p < 0.02$), and CEEE ($p < 0.02$). For $Ca_V1.2$, *r300* values varied from 0.73 ± 0.03 to 0.61 ± 0.04 (control) and from 0.51 ± 0.04 to 0.28 ± 0.03 (mibefradil). For $Ca_V1.2$ E462R, *r300* went from 0.48 ± 0.03 to 0.24 ± 0.03 (control) and from 0.29 ± 0.03 to 0.04 ± 0.03 (mibefradil). For CEEE, *r300* amounted to 0.49 ± 0.04 to 0.2 ± 0.06 (control) and from 0.27 ± 0.03 to 0.07 ± 0.04 (mibefradil). (*D–F*) Mibefradil (10 μM) had little effect on the inactivation kinetics of $Ca_V2.3$–like channels. For $Ca_V2.3$, *r300* values dropped from 0.05 ± 0.006 to 0.01 ± 0.004 (control) and from 0.06 ± 0.01 to 0.004 ± 0.003 (mibefradil). For EC(*IS1-6*)EEE, *r300* dropped from 0.11 ± 0.01 to 0.06 ± 0.01 (control) and from 0.14 ± 0.02 to 0.02 ± 0.01 (mibefradil). For EC(*AID*)EEE, *r300* dropped from 0.27 ± 0.01 to 0.16 ± 0.01 (control) and from 0.24 ± 0.03 to 0.09 ± 0.02 (mibefradil). Note that the differences observed at −10 mV for $Ca_V2.3$ and EC(*IS1-6*)EEE are not significant at $p < 0.1$. The *y*-axis scale is different for each graph. Paired Student *t*-tests were performed; $p < 0.0005$ (***), $p < 0.02$ (**), and $p < 0.1$ (*).

finity for CEEE with IC_{50} going from 68 ± 9 μM at 0 mV to 31 ± 4 μM at +20 mV ($n = 5$). In contrast, mibefradil affinity for $Ca_V1.2$ E462R, $Ca_V2.3$ R378E, EC(*IS1-6*)EEE, and $Ca_V2.3$ wild-type channels was not significantly affected by depolarization between 0 and +20 mV (*as shown*) and even between −10 and +30 mV (*results not shown*). Depolarization appeared to slightly increase mibefradil affinity for $Ca_V2.3$ R378E, but the larger variability of the data points prevents it from being statistically significant. Inhibition data points measured at 0 and +20 mV were not significantly different for $Ca_V1.2$ E462R, and were clearly indistinguishable for EC(*IS1-6*)EEE and $Ca_V2.3$ channels. Mibefradil inhibition of $Ca_V3.1$ and $Ca_V3.2$ channels was also reported to be insensitive to changes in membrane potential, an observation that was interpreted as reflecting the relatively

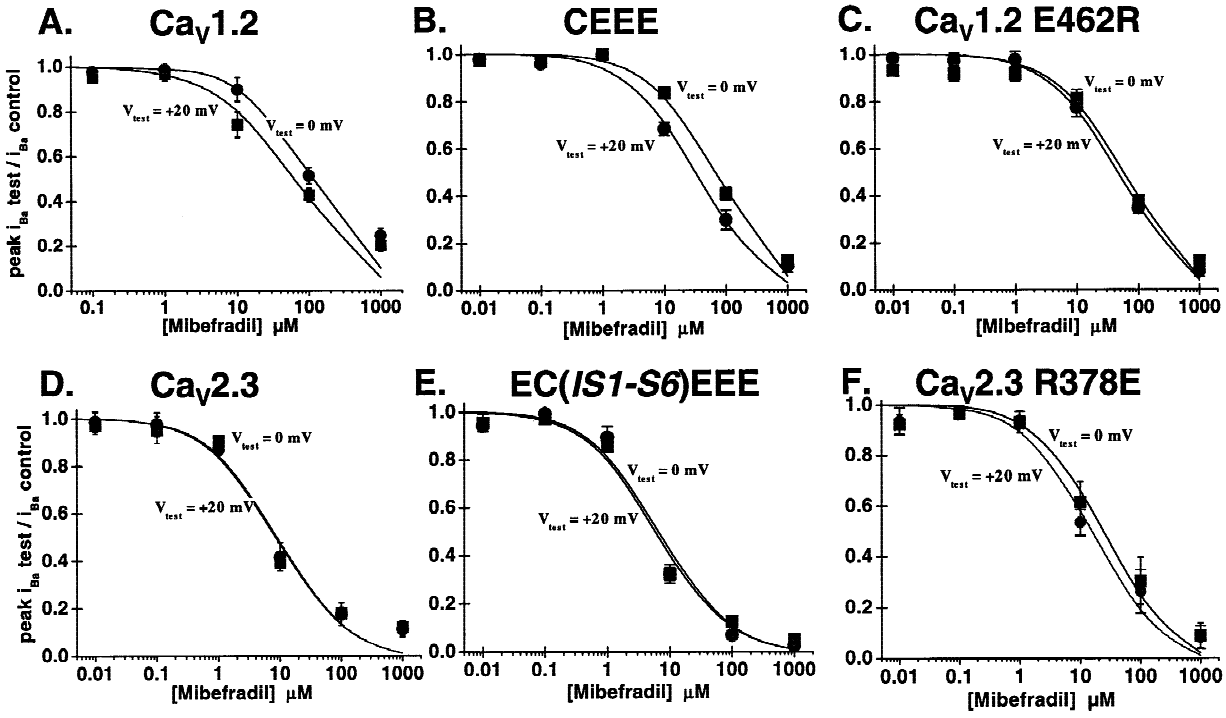

Fig. 7. Depolarization increased the affinity of $Ca_V1.2$ channels to mibefradil. The dose-response curves were measured at a fixed membrane potential of 0 or +20 mV. Peak currents recorded at these voltages in the presence of mibefradil were normalized to the peak current measured under control conditions. Paired measurements were made on 4–9 experiments. (*A–B*) Depolarization from 0 to +20 mV significantly increased the affinity of $Ca_V1.2$ and CEEE channels for mibefradil. For $Ca_V1.2$, IC_{50} decreased from 108 ± 21 μM at 0 mV to 64 ± 15 μM ($n = 7$) at +20 mV. For CEEE, IC_{50} dropped from 68 ± 9 μM at 0 mV to 31 ± 4 μM at +20 mV ($n = 5$). (*C–F*) In contrast, mibefradil affinity for $Ca_V1.2$ E462R, $Ca_V2.3$ R378E, EC(*IS1-6*)EEE, and $Ca_V2.3$ wild-type channels was not significantly affected by depolarization between 0 and +20 mV. The calculated IC_{50} values were as follows: 58 ± 7 μM at 0 mV and 47 ± 5 μM at +20 mV ($n = 6$) for $Ca_V1.2$ E462R; 8 ± 2 μM at 0 mV and 9 ± 2 μM at +20 mV ($n = 9$) for $Ca_V2.3$; 7 ± 1 μM at 0 mV and 6 ± 2 μM at +20 mV ($n = 3$) for EC(*IS1-6*)EEE; 31 ± 4 μM at 0 mV and 25 ± 6 μM at +20 mV ($n = 5$) for $Ca_V2.3$ R378E.

slow on- and off-rates of drug binding (Martin et al., 2000).

Discussion

Mibefradil Inhibition of Voltage-dependent Ca^{2+} Channels

Mibefradil has been reported to inhibit the three gene families of voltage-dependent calcium channels, including low-activated calcium channels such as T-type $Ca_V3.1$, $Ca_V3.2$, and $Ca_V3.3$ with $IC_{50} \approx 0.4-2$ μM (Lacinova et al., 2000a; Martin et al., 2000); high-voltage activated calcium channels $Ca_V2.1$ and $Ca_V2.3$ with $IC_{50} \approx 1–10$ μM (Bezprozvanny & Tsien, 1995; Jimenez et al., 2000) and L-type $Ca_V1.2$ with $IC_{50} \approx 20–100$ μM (Bezprozvanny & Tsien, 1995; Jimenez et al., 2000; Martin et al., 2000). In our hands, mibefradil inhibited $Ca_V1.2$ and $Ca_V2.3$ channels in a dose-dependent manner. $Ca_V2.3$ displayed a higher affinity for mibefradil with $IC_{50} = 8 \pm 2$ μM ($n = 9$) at $HP = -80$ mV and 33 ± 7 μM ($n = 4$) at $HP = -100$ mV. $Ca_V1.2$ channels were on average 10 times less sensitive, with an $IC_{50} = 108 \pm 21$ μM ($n = 7$) at $HP = -80$ mV and 288 ± 17 μM ($n = 3$) at $HP = -100$ mV. This observation is consistent with previous studies, whether recombinant channels were expressed with either β1, β2, and β3 subunits in oocytes (Bezprozvanny & Tsien, 1995) or in mammalian cells (Jimenez et al., 2000; Martin et al., 2000). Nonetheless, the dose-response curves were typically shifted to higher concentrations in the oocyte expression system, suggesting that mibefradil might not diffuse as freely through the oocyte membrane as it does through the mammalian one.

Voltage-dependent Inhibition of $Ca_V1.2$ and $Ca_V2.3$ Channels by Mibefradil

Voltage-dependent inhibition of high-voltage-activated Ca^{2+} channels by mibefradil has been first suggested from the increased potency of the drug at depolarized potentials (Bezprozvanny & Tsien, 1995) and most re-

cently inferred from experiments with $Ca_V1.2$, $Ca_V2.1$, and $Ca_V2.3$ channels heterologously expressed in the presence of β3-subunits known to promote voltage-dependent inactivation (Jimenez et al., 2000). Our experiments largely confirmed that mibefradil inhibits $Ca_V1.2$ and $Ca_V2.3$ channels in a voltage-dependent manner. Increasing channel availability by increasing the holding potential from −80 to −120 mV, decreased mibefradil affinity for $Ca_V1.2$ and $Ca_V2.3$ channels. This decrease was similar in both channel types, suggesting that inactivation enhanced their respective mibefradil affinity to a similar extent. Furthermore, mibefradil sped up inactivation kinetics of $Ca_V1.2$ channels as previously reported (Welling et al., 1995) whereas it failed to affect the inactivation kinetics of the faster $Ca_V2.3$ channels. Depolarization also increased the affinity of $Ca_V1.2$ channels to mibefradil, but had little effect on the inhibition of $Ca_V2.3$ wild-type and like channels.

Mibefradil failed to significantly alter the voltage-dependence of $Ca_V2.3$ inactivation, although it caused the $Ca_V1.2$ channel to inactivate at slightly more negative membrane potentials (a shift of −10 mV). In that latter case, however, it should be pointed out that under our experimental conditions (5-sec prepulses), $Ca_V2.1$ channel inactivation was not measured under true steady-state conditions and ≈20% of the channels had yet to inactivate. Although mibefradil altered more significantly the inactivation properties of the slow-inactivating $Ca_V1.2$ than the fast-inactivating $Ca_V2.3$ channels, both channels were inhibited in a state-dependent manner.

Mibefradil Locks $Ca_V1.2$ and $Ca_V2.3$ Channels into an Absorbing Inactivated State

Mibefradil significantly delayed $Ca_V1.2$ and $Ca_V2.3$ recovery from inactivation. This delayed recovery was observed for wild-type and mutant $Ca_V1.2$ and $Ca_V2.3$ channels alike. The mibefradil-induced delay in the onset of recovery from inactivation (Figs. 3 and 5) suggests that binding of the drug to the open state promotes channel transition into a slow and absorbing inactivated state (IOB) (*see* Fig. 9). Drug-induced delay in the onset of recovery from inactivation has also been reported for the inhibition of recombinant $Ca_V1.2$ channels by dihydropyridines and phenylalkylamines (Hering et al., 1997; Lacinova et al., 2000b). By analogy with sodium channel interaction with local anesthetics (Hockerman et al., 2000), slow recovery from inactivation may consequently have an important role in the action of Ca^{2+} antagonists.

Correlation between Fast Inactivation Kinetics and Mibefradil Affinity

The most compelling evidence in support of state-dependent inhibition was provided by the direct relationship between mibefradil affinity and the inactivation kinetics of wild-type and inactivation-modified $Ca_V1.2$ and $Ca_V2.3$ channels (*see* Fig. 8). Inactivation-altered mutants were produced within the I-II linker, which has recently emerged as a critical determinant of voltage-dependent inactivation in high-voltage-activated Ca^{2+} channels (Herlitze et al., 1997; Page et al., 1997; Stotz et al., 2000; Berrou et al., 2001; Parent et al., 2001). The slower $Ca_V1.2$ wild-type and $Ca_V1.2$ Q473K channels were found to display the lowest affinity for mibefradil. Intermediate inactivation kinetics for $Ca_V1.2$ E462K & E462R, and CEEE yielded intermediate IC_{50} (≈60 μM) for mibefradil. In particular, single-point mutations in the I-II linker at position E462 (either E462R or E462K) increased 1.8-fold the affinity of mibefradil for $Ca_V1.2$ channels. Mibefradil inhibition of chimera EC(*AID*)EEE and mutant $Ca_V2.3$ R378E were shown to occur around an IC_{50} value of 30 to 35 μM. The faster $Ca_V2.3$ and EC(*IS1-6*)EEE channels were the most potently inhibited by mibefradil with a $IC_{50} \approx 7$ μM. Interestingly, the correlation remained extremely good for the "normal-like" mutant $Ca_V1.2$ Q473K, which lies only a few residues away from E462 in the I-II linker, thus diminishing the possibility that nonspecific changes in the secondary structure accounted for the differences in mibefradil affinity. Hence, our results suggest that the macroscopic rate of transition to the inactivated state is a good predictor of mibefradil affinity for $Ca_V1.2$ and $Ca_V2.3$ chan-

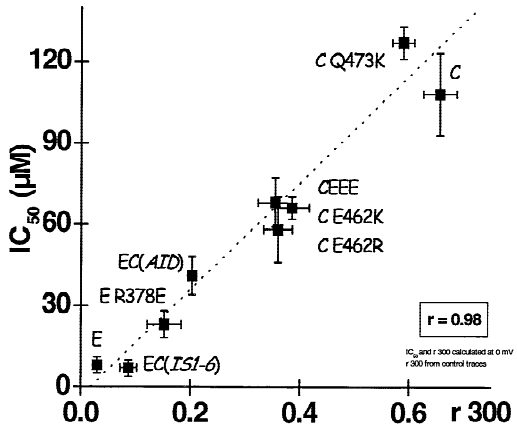

Fig. 8. Mibefradil affinity is correlated with inactivation kinetics. IC_{50} and *r300* were calculated here from the same set of data at a fixed V_m = 0 mV. The *r300* values were measured under control conditions before the addition of the drug to the bath. These values were *r300* = 0.03 ± 0.01 and IC_{50} = 8 ± 2 μM (n = 9) for $Ca_V2.3$; *r300* = 0.09 ± 0.01 and IC_{50} = 7 ± 1 μM (n = 3) for EC(*IS1-6*)EEE; *r300* = 0.33 ± 0.01 and IC_{50} = 41 ± 5 μM (n = 4) for EC(*AID*)EEE; *r300* = 0.49 ± 0.04 and IC_{50} = 68 ± 9 μM (n = 5) for CEEE; *r300* = 0.59 ± 0.03 and IC_{50} = 117 ± 11 μM (n = 3) for $Ca_V1.2$ Q473K; *r300* = 0.66 ± 0.03 and IC_{50} = 108 ± 21 μM (n = 7) for $Ca_V1.2$. In the figure, "*C*" stands for $Ca_V1.2$ and "*E*" stands for $Ca_V2.3$. The number of experiments varied between 4 and 9. The correlation coefficient r was 0.98 between IC_{50} values and inactivation kinetics.

nels. However, as measured under whole-cell conditions, the global rate of transition toward the inactivated state actually results from the net sum of the open (*O*) to closed (*C*) as well as the *O* to inactivated (*I*) transitions (*see* Fig. 9 and discussion below).

Although it is well established that local anesthetics and antiarrhythmics exert their therapeutic effects by preferentially altering the inactivated state of voltage-dependent channels, only a few groups have specifically investigated the change in drug affinity experienced by inactivated-altered Ca^{2+} channels. In this regard, the correlation between inactivation kinetics and drug affinity has been extensively characterized in $Ca_V2.1$ wild-type and mutant channels for the members of the phenylalkylamine, benzothiazepine, or dihydropyridine compound families (Hering et al., 1997). In contrast, few data exist to document the consequence of inactivation-altering mutations on the channel sensitivity to mibefradil and they appear to be conflicting. Point mutations in the IVS6 region were shown to alter inactivation kinetics without modifying the channel affinity for mibefradil (Aczel et al., 1998). Nonetheless, the observation that a single point mutation in the I-II linker of the α1A-b splice variant of $Ca_V2.1$ channels (Bourinet et al., 1999) simultaneously decreased the channel inactivation kinetics and the channel affinity for mibefradil (Jimenez et al., 2000) agrees with our own data.

Molecular Mechanisms of Ca^{2+} Channel Inhibition by Mibefradil

Ion-channel inhibition by organic blockers is determined by the drug binding to the protein itself as well as the accessibility of the drug to the channel protein. As elegantly reviewed by Hering and coll. (Hering et al., 1998), one of the major challenges facing the elucidation of the molecular mechanisms underlying ion-channel modulation by pharmacological agents is to distinguish between these two processes. The problem is compounded by the observation that mutations in the DHP receptor binding site will also alter the rate of inactivation in $Ca_V1.2$ channels (Hering et al., 1997; Hockerman et al., 1997). Conversely, point mutations that alter the pathway by which drugs gain access will also mimic changes in the receptor affinity for the drugs (Hering et al., 1998). Such molecular mechanism has been formalized under the "guarded receptor model" (Starmer & Grant, 1985) which predicts that the drug affinity will be modulated by the ion-channel gating process. Herein, the effects of mibefradil were studied using previously characterized inactivation-altered mutants (Bernatchez et al., 2001; Berrou et al., 2001). As mibefradil has been shown to inhibit all three gene families of Ca^{2+} channels with a higher affinity for faster-inactivating channels, it is tempting to speculate that the inactivation-gating structures of these channels control the drug access.

To provide some insight into the molecular mechanism, we solved the "gated access" model that was proposed to account for the interaction of pharmacological agents with Ca^{2+} channels according to Hering and coll. (Hering et al., 1998). The five-state kinetic model is detailed in Fig. 9A and the analytical solution appears in the Appendix. In this model, mibefradil access to its receptor site is impeded in the closed conformation of the channel. Depolarization enables mibefradil to interact with its receptor. Channels that display fast inactivation gating are predicted to be more efficiently inhibited because the drug is trapped in the pore. Hence, it is predicted that organic blockers will display a reduced affinity to slower-inactivating channels.

The model herein described is minimalist since channel kinetics in the absence of the drug are described by a three-state coupled scheme whereby channels have to transit through the open state (*O*) to become inactivated (*I*). For simplicity's sake, direct transitions from the closed state to the inactivated state, believed to occur in $Ca_V2.3$ channels (Patil, Brody & Yue, 1998) were not included. Furthermore, transitions to the inactivated state (*I*) and the inactivated-open-blocked state (*IOB*) are considered irreversible for this analysis.

Our model favors the interaction of mibefradil with the channel open state, although a small interaction between mibefradil and the inactivated state of $Ca_V1.2$ channels cannot be entirely ruled out (Bezprozvanny & Tsien, 1995) as suggested by the mibefradil-induced shift of −8 mV in the voltage-dependence of inactivation in these channels. However, it should be pointed out that dominant drug binding to the inactivated state could not adequately reproduce our data at least within the limits of the tightly coupled inactivation model we used.

To successfully account for our data, channels with fast inactivation kinetics should display a higher affinity to mibefradil. Whole-cell inactivation kinetics could be made faster by increasing *k4* or decreasing *k2*. The observed relationship between inactivation gating and mibefradil affinity argues, however, strongly for a fast inactivation process controlled by *k2* (e.g., the rate of deactivation). Fast inactivation kinetics as controlled by a slow deactivation rate will more efficiently trap the drug into the channel than slow inactivation kinetics. In contrast, a high deactivation rate is predicted to limit the time spent in the open state thus reducing the accessibility to the inactivation state causing slow inactivation kinetics and concomitantly decreasing the efficiency of the drug binding. Hence, according to the proposed model, increasing mibefradil concentration will prevent the deactivation of the channel. The assumption that mibefradil affects the channel-deactivation rate remains to be verified at the single-channel level. Nevertheless, similar models, where transitions back to the resting state are reduced after the drug binding to the channel open-

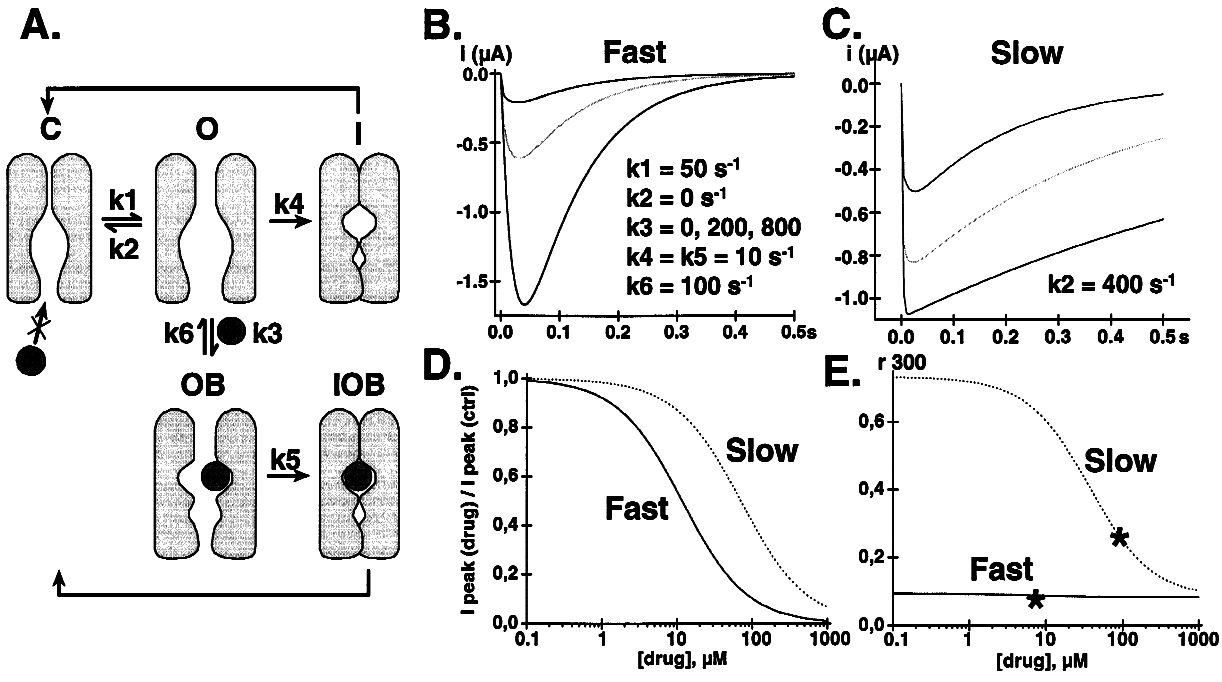

Fig. 9. Kinetic model of mibefradil interaction with slow- and fast-inactivating channels. (*A*) A proposed model for mibefradil interaction with high-voltage-gated Ca^{2+} channels that could account for the higher affinity of fast-inactivating channels. Activation and inactivation are shown as coupled processes whereby most channels have to transit through the open state (*O*) to become inactivated (*I*). Mibefradil access (symbolized by the grey ball) is impeded in the closed state (*C*) but is facilitated in the open conformational state (*O*) where it interacts with its receptor site (*OB*). Channels locked in the open-blocked state (*OB*) become non conducting and eventually accumulate into an absorbing inactivated open-blocked state (*IOB*) that is kinetically indistinguishable from the inactivated state (*I*). The *IOB* state, however, must be introduced to account for the slower kinetics of recovery from inactivation measured in the presence of the drug. In our model, channels that display fast inactivation gating are predicted to be more strongly inhibited because they exhibit a larger probability to be in the open state, thus enhancing the efficiency of the drug binding at similar concentrations. In contrast, mibefradil will display a reduced affinity to slower-inactivating channels because the latter spend relatively little time in the open state thus severely limiting the transition to the inactivated state as well as drug binding. (*B*) The time course of whole-cell current traces for the faster channel was simulated using the analytical solution to the model shown in *A* with the following time constants: $k1 = 50\ sec^{-1}$; $k2 = 0.4\ sec^{-1}$; $k4 = k5 = 10\ sec^{-1}$; and $k6 = 100\ sec^{-1}$ with $P(closed) = 1$ at time $t = 0$ using $k3 = k3'[drug]$ where $k3' = 10\ \mu M^{-1}\ sec^{-1}$ and the drug concentration is given in μM. The three traces were obtained for three values of *k3* with mibefradil concentrations of 0, 20, and 80 μM from bottom to top. The current traces were computed with $I = NiP(open)$, where both *N* (number of channels) and *i* (unitary current) were adjustable parameters. For all simulations, $k_2 < k_1$ for fast-inactivating channels and $k_2 > k_1$ for slow-inactivating ones. It was also assumed that $k4 \approx k5$, meaning that the transition rate from the open (*O*) to the inactivated state is unaffected by the presence of the drug. (*C*) Time course of whole-cell current traces for the slower channel with the following time constants: $k1 = 50\ sec^{-1}$; $k2 = 400\ sec^{-1}$; $k4 = k5 = 10\ sec^{-1}$; and $k6 = 100\ sec^{-1}$. The three traces were obtained for 0, 20, and 80 μM mibefradil from bottom to top. (*D*) The model predicts that the dose-response curves will shift toward higher concentrations for slow inactivating channels (dotted line) as compared to the fast ones (solid line). As predicted by the model, the IC_{50} would be ≈100 μM for the slower channel and ≈10 μM for the faster one. (*E*) The model further predicts that mibefradil will affect more significantly the kinetics of slow-inactivating channels. The inactivation kinetics were estimated as a function of the drug concentration. The *r300* ratios were calculated from whole-cell current traces for *k3* values ranging from $0.1\ sec^{-1}$ to $10^3\ sec^{-1}$. As seen, the inactivation kinetics of the slow channel (dotted line) are predicted to be more strongly accelerated by increasing doses of mibefradil than the inactivation of the fast channel (solid line). The asterisks point to the predicted IC_{50} for mibefradil since the changes in inactivation kinetics shown in Fig. 6 were calculated using mid-inhibitory concentrations. Simulations were performed for $V_m = 0$ mV by solving the Fourier integral of the inverse matrix of the rates of transitions (Roux & Sauve, 1985) using Mathematica® (Wolfram Corporation).

state, have been successfully used to explain use-dependent block of native, recombinant, and mutants $Ca_V1.2$ channels by benzothiazepines, dihydropyridines, and phenylalkylamines (Armstrong, 1971; Bean, 1984; Kass & Sanguinetti, 1984; Hering et al., 1997).

Simulations were performed using the analytical solution of this model with rate constants that could qualitatively reproduce the whole-cell inactivation kinetics (Fig. 9*B–E*). Panels *B* and *C* reproduced the predicted time course of whole-cell Ba^{2+} traces for a fast (Fig. 9*B*) and for a slow (Fig. 9*C*) channel at three different mibefradil concentrations (0, 20 and 80 μM) using $V_m = 0$ mV. The predicted dose-response curve is shown to lay at higher concentrations for the slow-inactivating channels (*compare* Figs. 4, 8, 9*D*). Inactivation kinetics of slow channels are also expected to be more significantly influenced by the drug concentration (*compare* Figs. 6 and 9*E*). Hence, the "gated-access" model could account

for the correlation between fast inactivating kinetics and higher mibefradil affinity as well as for the mibefradil-induced acceleration of inactivation kinetics that was more prominently featured in slow-inactivating $Ca_V1.2$ and CEEE channels.

Whereas this kinetic model remains the simplest possible one to account for our data, introducing reversible transitions and/or including additional closed and inactivated states to the model would enhance its predictive power. In essence, we believe that these modifications would not alter the fundamental results of our simulations, fast inactivation kinetics enhances mibefradil affinity to high-voltage-activated Ca^{2+} channels. Although our data are compatible with a "guarded receptor" mechanism, we cannot completely rule out that the molecular determinants of inactivation targeted in our study (e.g., the I-II linker) are also involved in the mibefradil binding site.

We are grateful to Drs. J.P. Clozel and M.D. Payet for the generous gift of mibefradil. We thank Ms. Julie Verner for expert oocyte preparation and culture; Mr. Claude Gauthier for artwork; and colleagues for discussions. L.P. is a Senior scholar from the "Fonds de la Recherche en Santé du Québec". This work was performed with grant MT13390 from the Canadian Research Institutes MT13390 and with a grant from the Canadian Heart & Stroke Foundation to L.P.

References

Aczel, S., Kurka, B., Hering, S. 1998. Mechanism of voltage- and use-dependent block of class A Ca^{2+} channels by mibefradil. *Br. J. Pharmacol.* **125:**447–454

Armstrong, C.M. 1971. Interaction of tetraethylammonium ion derivatives with the potassium channels of giant axons. *J. Gen. Physiol.* **58:**413–437

Arnoult, C., Villaz, M., Florman, H.M. 1998. Pharmacological properties of the T-type Ca^{2+} current of mouse spermatogenic cells. *Mol. Pharmacol.* **53:**1104–1111

Bean, B.P. 1984. Nitrendipine block of cardiac calcium channels: high-affinity binding to the inactivated state. *Proc. Natl. Acad. Sci. USA* **81:**6388–6392

Bernatchez, G., Berrou, L., Benakezouh, Z., Ducay, J., Parent, L. 2001. Role of Repeat I in the fast inactivation kinetics of the $Ca_V2.3$ channel. *Bioch. Biophys. Acta* **1514:**217–229

Bernatchez, G., Talwar, D., Parent, L. 1998. Mutations in the EF-hand motif of the cardiac α_{1C} calcium channel impair the inactivation of barium currents. *Biophys. J.* **75:**1727–1739

Berrou, L., Bernatchez, G., Parent, L. 2001. Molecular determinants of inactivation within the I-II linker of α1E ($Ca_V2.3$) Ca^{2+} channels. *Biophys. J.* **80:**215–228

Bezprozvanny, I., Tsien, R.W. 1995. Voltage-dependent blockade of diverse types of voltage-gated Ca^{2+} channels expressed in *Xenopus* oocytes by the Ca^{2+} channel antagonist mibefradil (Ro 40-5967). *Mol. Pharmacol.* **48:**540–599

Bourinet, E., Soong, T.W., Sutton, K., Slaymaker, S., Mathews, E., Monteil, A., Zamponi, G.W., Nargeot, J., Snutch, T.P. 1999. Splicing of α1A subunit gene generates phenotypic variants of P- and Q-type calcium channels. *Nat. Neurosci.* **2:**407–415

Castellano, A., Wei, X., Birnbaumer, L., Perez-Reyes, E. 1993. Cloning and expression of a third calcium channel β subunit. *J. Biol. Chem.* **268:**3450–3455

Cens, T., Restituito, S., Galas, S., Charnet, P. 1999. Voltage and calcium use the same molecular determinants to inactivate calcium channels. *J. Biol. Chem.* **274:**5483–5490

Chouabe, C., Drici, M.D., Romey, G., Barhanin, J., Lazdunski, M. 1998. HERG and KvLQT1/IsK, the cardiac K^+ channels involved in long QT syndromes, are targets for calcium channel blockers. *Mol. Pharmacol.* **54:**695–703

Clozel, J.P., Banken, L., Osterrieder, W. 1989. Effects of Ro 40-5967, a novel calcium antagonist, on myocardial function during ischemia induced by lowering coronary perfusion pressure in dogs: comparison with verapamil. *J. Cardiovasc. Pharmacol.* **14:**713–721

Clozel, J.P., Ertel, E.A., Ertel, S.I. 1997. Discovery and main pharmacological properties of mibefradil (Ro 40-5967), the first selective T-type calcium channel blocker. *J. Hypert.* **15:**S17–S25,S17–S25

Eller, P., Berjukov, S., Wanner, S., Huber, I., Hering, S., Knaus, H.G., Toth, G., Kimball, S.D., Striessnig, J. 2000. High affinity interaction of mibefradil with voltage-gated calcium and sodium channels. *Br. J. Pharmacol.* **130:**669–677

Esneu, M., Gallo-Payet, N., Payet, M.D. 1998. Mibefradil, a T-type calcium channel antagonist in Y1 cells. *Endocr. Res.* **24:**449–454

Gomora, J.C., Xu, L., Enyeart, J.A., Enyeart, J.J. 2000. Effect of mibefradil on voltage-dependent gating and kinetics of T-type Ca^{2+} channels in cortisol-secreting cells. *J. Pharmacol. Exp. Ther.* **292:**96–103

Hering, S., Aczel, S., Kraus, R.L., Berjukow, S., Striessnig, J., Timin, E.N. 1997. Molecular mechanism of use-dependent calcium channel block by phenylalkylamines: role of inactivation. *Proc. Natl. Acad. Sci. USA* **94:**13323–13328

Hering, S., Berjukow, S., Aczel, S., Timin, E.N. 1998. Ca^{2+} channel block and inactivation: common molecular determinants. *Trends Pharmacol. Sci.* **19:**439–443

Herlitze, S., Hockerman, G.H., Scheuer, T., Catterall, W.A. 1997. Molecular determinants of inactivation and G protein modulation in the intracellular loop connecting domains I and II of the calcium channel α_{1A} subunit. *Proc. Natl. Acad. Sci. USA* **94:**1512–1516

Hille, B. 1977. Local anesthetics: hydrophilic and hydrophobic pathways for the drug-receptor reaction. *J. Gen. Physiol.* **69:**497–515

Hille, B. 1992. Ionic Channels of Excitable Membranes, Sunderland MA

Hockerman, G.H., Dilmac, N., Scheuer, T., Catterall, W.A. 2000. Molecular Determinants of Diltiazem Block in Domains IIIS6 and IVS6 of L-type Ca^{2+} Channels. *Mol. Pharmacol.* **58:**1264–1270

Hockerman, G.H., Johnson, B.D., Abbott, M.R., Scheuer, T., Catterall, W.A. 1997. Molecular determinants of high affinity phenylalkylamine block of L-type calcium channels in transmembrane segment IIIS6 and the pore region of the α1 subunit. *J. Biol. Chem.* **272:**18759–18765

Jimenez, C., Bourinet, E., Leuranguer, V., Richard, S., Snutch, T.P., Nargeot, J. 2000. Determinants of voltage-dependent inactivation affect Mibefradil block of calcium channels. *Neuropharmacology* **39:**1–10

Kass, R.S., Sanguinetti, M.C. 1984. Inactivation of calcium channel current in the calf cardiac Purkinje fiber. Evidence for voltage- and calcium-mediated mechanisms. *J. Gen. Physiol.* **84:**705–726

Klugbauer, N., Marais, E., Lacinova, L., Hofmann, F. 1999. A T-type calcium channel from mouse brain. *Pfluegers Arch.* **437:**710–715

Lacinova, L., Klugbauer, N., Hofmann, F. 2000a. Regulation of the calcium channel α1G subunit by divalent cations and organic blockers. *Neuropharm.* **39:**1254–1266

Lacinova, L., Klugbauer, N., Hofmann, F. 2000b. State- and isoform-dependent interaction of isradipine with the α1C L-type calcium channel. *Pfluegers Arch.* **440:**50–60

Lacinova, L., Welling, A., Bosse, E., Ruth, P., Flockerzi, V., Hofmann, F. 1995. Interaction of Ro 40-5967 and verapamil with the stably expressed α1-subunit of the cardiac L-type calcium channel. *J. Pharmacol. Exp. Ther.* **274:**54–63

Liu, J.H., Bijlenga, P., Occhiodoro, T., Fischer-Lougheed, J., Bader, C.R., Bernheim, L. 1999. Mibefradil (Ro 40-5967) inhibits several Ca^{2+} and K^+ currents in human fusion-competent myoblasts. *Br. J. Pharmacol.* **126:**245–250

Martin, R.L., Lee, J.H., Cribbs, L.L., Perez-Reyes, E., Hanck, D.A. 2000. Mibefradil block of cloned T-type calcium channels *J. Pharmacol. Exp. Ther.* **295:**302–308

McNaughton, N.C., Warre, R., Cooper, D.G., Nasir, S., Ranson, J.L., Randall, A. 2000. Potent inhibition of a recombinant low voltage-activated Ca^{2+} channel by SB-209712. *Eur. J. Pharmacol.* **407:**53–60

Mishra, S.K., Hermsmeyer, K. 1994. Inhibition of signal Ca^{2+} in dog coronary arterial vascular muscle cells by Ro 40-5967. *J. Cardiovasc. Pharmacol.* **24:**1–7

Monteil, A., Chemin, J., Bourinet, E., Mennessier, G., Lory, P., Nargeot, J. 2000. Molecular and functional properties of the human α1G subunit that forms T-type calcium channels. *J. Biol. Chem.* **275:**6090–6100

Page, K.M., Stephens, G.J., Berrow, N.S., Dolphin, A.C. 1997. The intracellular loop between domains I and II of the B-type calcium channel confers aspects of G-protein sensitivity to the E-type calcium channel. *J. Neurosci.* **17:**1330–1338

Parent, L., Bernatchez, G., Berrou, L., Benakezouh, Z., Ducay, J. 2001. Fast inactivation of the $Ca_V2.3$ channel: role of the I-II linker. *Biophys. J.* **80:**620a

Parent, L., Gopalakrishnan, M. 1995a. Glutamate substitution in repeat IV alters divalent and monovalent cation permeation in the heart Ca^{2+} channel. *Biophys. J.* **69:**1801–1813

Parent, L., Gopalakrishnan, M., Lacerda, A.E., Wei, X., Perez-Reyes, E. 1995b. Voltage-dependent inactivation in a cardiac-skeletal chimeric calcium channel. *FEBS Lett.* **360:**144–150

Parent, L., Schneider, T., Moore, C.P., Talwar, D. 1997. Subunit regulation of the human brain α_{1E} calcium channel. *J. Membrane Biol.* **160:**127–140

Patil, P.G., Brody, D.L., Yue, D.T. 1998. Preferential closed-state inactivation of neuronal calcium channels. *Neuron* **20:**1027–1038

Perchenet, L., Benardeau, A., Ertel, E.A. 2000a. Pharmacological properties of $Ca_V3.2$, a low voltage-activated Ca^{2+} channel cloned from human heart. *Naunyn Schmiedebergs Arch. Pharmacol.* **361:**590–599

Perchenet, L., Clement-Chomienne, O. 2000b. Characterization of mibefradil block of the human heart delayed rectifier hKv1.5 *J. Pharmacol. Exp. Ther.* **295:**771–778

Peterson, B.Z., Lee, J.S., Mulle, J.G., Wang, Y., de, L.M., Yue, D.T. 2000. Critical determinants of Ca^{2+}-dependent inactivation within an EF-hand motif of L-type Ca^{2+} channels. *Biophys. J.* **78:**1906–1920

Protas, L., Robinson, R.B. 2000. Mibefradil, an I(Ca,T) blocker, effectively blocks I(Ca,L) in rabbit sinus node cells. *Eur. J. Pharmacol.* **401:**27–30

Roux, B., Sauve, R. 1985. A general solution to the time interval omission problem applied to single channel analysis. *Biophys. J.* **48:**149–158

Sambrook, J., Fritsch, E.F., and Maniatis, T. 1989. *Molecular Cloning: A Laboratory Manual* (*2nd ed*), Cold Spring Harbor Laboratory, Cold Spring Harbor, New York

Starmer, C.F., Grant, A.O. 1985. Phasic ion channel blockade. A kinetic model and parameter estimation procedure. *Mol. Pharmacol.* **28:**348–356

Stotz, S.C., Hamid, J., Spaetgens, R.L., Jarvis, S.E., Zamponi, G.W. 2000. Fast inactivation of voltage-dependent calcium channels: A hinged-lid mechanism. *J. Biol. Chem.* **275:**24575–24582

Todorovic, S.M., Lingle, C.J. 1998. Pharmacological properties of T-type Ca^{2+} current in adult rat sensory neurons: effects of anticonvulsant and anesthetic agents. *J. Neurophysiol.* **79:**240–252

Welling, A., Lacinova, L., Donatin, K., Ludwig, A., Bosse, E., Flockerzi, V., Hofmann, F. 1995. Expression of the L-type calcium channel with two different β-subunits and its modulation by Ro 40-5967. *Pfluegers Arch.* **429:**400–411

Williams, M.E., Feldman, D.H., McCue, A.F., Brenner, R., Velicelebi, G., Ellis, S.B., Harpold, M.M. 1992. Structure and functional expression of α_1, α_2, and β subunits of a novel human neuronal calcium channel subtype. *Neuron* **8:**71–84

Williams, M.E., Washburn, M.S., Hans, M., Urrutia, A., Brust, P.F., Prodanovich, P., Harpold, M.M., Stauderman, K.A. 1999. Structure and functional characterization of a novel human low-voltage activated calcium channel. *J. Neurochem.* **72:**791–799

Wu, S., Zhang, M., Vest, P.A., Bhattacharjee, A., Liu, L., Li, M. 2000. A mibefradil metabolite is a potent intracellular blocker of L-type Ca^{2+} currents in pancreatic beta-cells. *J. Pharmacol. Exp. Ther.* **292:**939–943

Yarov-Yarovoy, V., Brown, J., Sharp, E.M., Clare, J.J., Scheuer, T., Catterall, W.A. 2001. Molecular determinants of voltage-dependent gating and binding of pore-blocking drugs in transmembrane segment IIIS6 of the Na^+ channel α subunit. *J. Biol. Chem.* **276:**20–27

Appendix

Let us consider a minimal kinetic model in which a drug (*D*) binds to the an open (*O*) channel leading to an open-block (*OB*) state. In the absence of the drug, the channel kinetic behavior is described by a simple closed (*C*), open (*O*) and inactivated (*I*) state model. The binding of the drug to the open channel is assumed to be reversible at a rate given by *k6*, but the model does not allow for reversibility of the inactivated/open-block state (*IOB*) to the *OB* state.

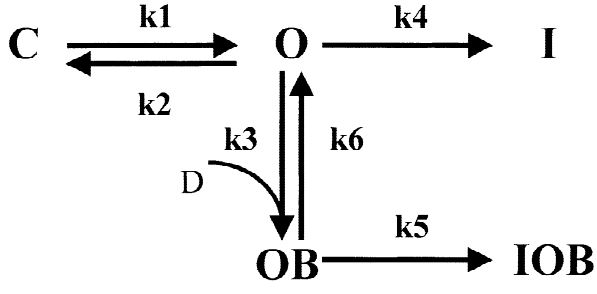

According to this scheme, the probability for the channel to be open (state *O*) at time *t*, knowing that it was closed at $t = 0$ is given by:

$$P(open) = \frac{k1(k5 + k6 - \omega_1)}{(\omega_1 - \omega_2)(\omega_1 - \omega_3)} \exp^{-\omega_1 t} + \frac{k1(k5 + k6 - \omega_2)}{(\omega_2 - \omega_1)(\omega_2 - \omega_3)} \exp^{-\omega_2 t} + \frac{k1(k5 + k6 - \omega 3)}{(\omega_3 - \omega_1)(\omega_3 - \omega_2)} \exp^{-\omega 3 t}$$

where ω_i with $1 < i < 3$ are solutions of

$$(\omega_i - k5 - k6)\ (\omega_i - x1)\ (\omega_i - x2) - k3k6(\omega_i - k1) = 0$$

for $x1$ and $x2$ given by:

$$x1 + x2 = k1 + k2 + k3 + k4$$

and

$$x1x2 = k1(k3 + k4)$$

Under conditions where the drug-binding to the channel is poorly reversible ($k6 \rightarrow 0$), the equation for $P(open)$ reduces to a summation of two exponential functions, with time constants corresponding to *x1* and *x2* respectively.